

THESIS

PRODUCTIVITY AND PHENOLOGY IN A PROCESS-DRIVEN CARBON CYCLE MODEL

Submitted by

Michael J. Cheeseman

Department of Atmospheric Science

In partial fulfillment of the requirements

For the Degree of Master of Science

Colorado State University

Fort Collins, Colorado

Fall 2018

Master's Committee:

Advisor: Scott Denning

Co-Advisor: Chris O'Dell

Libby Barnes

Julia Klein

Copyright by Michael J. Cheeseman 2018

All Rights Reserved

ABSTRACT

PRODUCTIVITY AND PHENOLOGY IN A PROCESS-DRIVEN CARBON CYCLE MODEL

The carbon cycle is a major source of uncertainty in predicting future climate, especially with regard to changes in the terrestrial biosphere. One obstacle in predicting the sources and sinks of the carbon cycle is accurately predicting phenological transitions of the terrestrial biosphere with a global process-driven model. We hypothesize that the terrestrial biosphere and its phenological transitions can be simulated using a set of universal biological strategies and a simple set of plant functional types in the Simple Biosphere (SiB4) model. In order to test our hypothesis, we compare the SiB4 output to a suite of satellite observations of the terrestrial biosphere including solar induced fluorescence (SIF) from the Orbiting Carbon Observatory (OCO-2), MODIS-based LAI, and AVHRR-based NDVI. Our first analysis compares modeled canopy SIF to aggregated satellite observed SIF over different biomes. We find that the model consistently over predicts pixel-scale SIF. Modeled SIF over evergreen needleleaf forests has an especially high bias during the winter. Our second analysis compares modeled and observed phenology over different regions around the globe. We find that SiB4 is generally successful in simulating growing season onset, but often simulates late senescence, especially in grasslands. We also find that SiB4 simulates crops well in the United States but fails to properly predict the planting and harvesting time of crops in other regions, especially the developing world.

ACKNOWLEDGEMENTS

I would like to thank my advisors Scott Denning and Chris O'Dell, as well as the rest of my research group for their guidance. I also want to thank my family and friends for supporting me as I aspire towards my research goals.

I would also like to thank the OCO-2 Science Team and the DOE Environmental System Science program for funding this work.

DEDICATION

I would like to dedicate this thesis to Nancy and John for making all of this possible.

TABLE OF CONTENTS

ABSTRACT	ii
ACKNOWLEDGEMENTS	iii
DEDICATION	iv
LIST OF TABLES	vi
LIST OF FIGURES	vii
Chapter 1 Introduction	1
1.1 Terrestrial Biosphere	1
1.2 What is phenology?	1
1.3 What is Solar Induced Fluorescence?	4
1.4 Testing a terrestrial biosphere model	6
Chapter 2 Methods	8
2.1 The SiB4 model	8
2.2 Observation datasets	12
2.3 Model SIF scaling from canopy to the landscape	15
2.4 Choosing geographic regions for analysis	15
2.5 Determining the timing of phenological transitions	17
Chapter 3 Results	20
3.1 SIF pixel-scale analysis	20
3.2 Phenology	24
3.2.1 Deciduous broadleaf forests	24
3.2.2 Tropical and sub-tropical grasslands	26
3.2.3 Agricultural regions	30
3.2.4 Tibetan Plateau	33
3.2.5 Boreal forests and grasslands	35
3.2.6 Evergreen broadleaf forests	35
Chapter 4 Discussion and Conclusions	37
Bibliography	41

LIST OF TABLES

2.1	Plant functional types	9
2.2	IGBP Land Classifications	14
2.3	Regional PFT Coverage	17

LIST OF FIGURES

1.1	Comparisons of SIF and gridded GPP	5
2.1	SiB4 model description	12
2.2	Map of research regions	16
2.3	Diagram of how phenology was captured	19
3.1	SIF canopy to pixel scaling	23
3.2	North American deciduous broadleaf forest phenology	26
3.3	South American grassland phenology	28
3.4	Northern Australia grassland phenology	29
3.5	African Sahel grassland phenology	30
3.6	North American agricultural phenology	32
3.7	Indian agricultural phenology	33
3.8	Tibetan Plateau phenology	34
3.9	Average seasonal SIF in boreal environments	35
3.10	Average seasonal SIF in evergreen broadleaf forests	36

Chapter 1

Introduction

1.1 Terrestrial Biosphere

The terrestrial biosphere removes approximately a quarter of anthropogenic CO₂ emissions from the atmosphere every year, slowing the rate of climate change [1]. Therefore, understanding the interactions of the terrestrial biosphere and the atmosphere, and how those interactions may change with rising CO₂, is crucial to projecting future climate. There are feedbacks in the terrestrial biosphere, some poorly understood [2], that have large implications on the rate of atmospheric CO₂ increase. The feedbacks of the terrestrial biosphere are the result of both the direct effect of increasing CO₂ on photosynthesis and the effect climate change has on photosynthesis, respiration, and disturbance [3]. Changes in photosynthesis and respiration, as well as the resulting change in vegetation seasonality, are part of a field of research known as phenology.

1.2 What is phenology?

Phenology is “the study of the timing of recurring biological events, the causes of their timing with regard to biotic and abiotic forces and the interactions among phases of the same or different species” [4]. In this paper we focus on phenological transitions, which “drive the seasonal progression of vegetation through stages of dormancy, active growth, and senescence” [5]. Phenological transitions can be easily observed in some environments, such as deciduous broadleaf forests. Trees produce buds in spring, create full canopies of leaves by summer, and then the leaves fall off in autumn resulting in barren trees over winter. However, phenological transitions are harder to understand and predict in other environments, such as tropical and evergreen forests. There, visible signs of these transitions and the factors that are driving them, are less easily observed [5]. In the past, phenology as a scientific field was often considered a study for amateurs, completed by individuals or families in their local ecosystems. One such amateur was the great

Henry David Thoreau [6]. Only in the last couple decades has phenology emerged as a critical aspect of carbon cycle research [7]. The shift began once scientists noticed that plant phenology could be used to track ecosystem response to inter-annual variability in weather, as well as long term impacts of climate change [8–10]. As the body of phenological research grew, its importance grew more evident. By dictating the timing of transitions in vegetation function and structure, phenology affects biological and physical processes from microscopic to global scales. Phenology is a factor in the survival and fitness of both plant and animal species, thereby affecting the gene pool of regional ecosystems [11–13]. Changes in phenology can affect both human health, by influencing the transport of allergens and disease, and land management practices such as agriculture, forestry, and invasive species control [7]. Phenology can also alter the larger climate system by influencing the exchange of mass, energy, moisture, and momentum between the biosphere and the atmosphere [5, 14]. A longer growing season, for example, can alter physical processes such as turbulence, albedo, and latent and sensible heat flux. It can also affect gas exchange processes such as the formation of BVOCs [15]. Changes in phenology can also change the carbon storage of regional ecosystems, which can influence the balance of natural carbon sources and sinks [15].

The majority of past phenological research has focused on drivers of spring phenology and how it may respond to climate change. A warming climate has been linked to earlier spring growth, earlier arrival of migratory birds and earlier emergence of migratory insects [16]. Early spring leaf-out, in combination with forest fuel build-up and a warming climate, have been linked to increased wildfires in drought stressed regions by enhancing soil and vegetation water depletion [17]. Autumn phenology is often the recipient of less attention by researchers, despite holding crucial biological events such as leaf senescence, fruit ripening, and bud formation [16]. It is still unclear in what circumstances leaf senescence will be advanced or delayed in a warming climate [7, 18], because it will depend on species-specific responses to environmental changes [19, 20]. Long-term observations suggest, however, that leaf senescence is delayed on average due to rising temperatures [21, 22]. Using prognostic models that can accurately describe global phenology is

crucial towards predicting how the terrestrial biosphere will change and interact with a warming climate [18, 23, 24].

Correctly modeling phenology has proven elusive, however [7]. Validation of modeled phenology is difficult because satellite based estimates of phenology often contradict each other and in situ estimates [25, 26]. Furthermore, there is a great dearth of biome-scale ground estimates of phenology [26]. In order to observe vegetation processes and phenology at a regional scale remote sensing derived vegetation indices (VI) have been developed. The normalized difference vegetation index (NDVI) has been one of the most commonly used products for phenological research [25, 27–30]. This product can be derived from multiple sensors such as the Advanced Very High Resolution Radiometer (AVHRR) and Moderate Resolution Imaging Spectroradiometer (MODIS). These products are highly noisy due to cloud cover, surface characteristics, and atmospheric conditions. They can also have missing information, spatially and temporally, due to snow, clouds, smoke, and other light scattering features [31]. Higher level products such as the MODIS-based leaf area index (LAI) were developed by coupling MODIS reflectances with a radiative transfer model in order to derive information about the vegetation canopy. This adds another layer of uncertainty due to poorly constrained radiative transfer model physics [18].

Satellite data often has coarse resolution, making it difficult to differentiate fine scale features or represent heterogeneity within single pixels (i.e. besides vegetation, other surfaces such as water, man-made objects, bare ground, affect spectral reflectance) and can make interpretation and validation of phenological estimates difficult. For example Churkina et al. [32] found that NDVI indicates a longer season than flux tower observations but this may be due to differences in scale between tower measurements and satellite pixels [33]. Peñuelas et al. [15] found, however, that coarse resolution data of phenology may be more beneficial to educating biosphere models due to the coarse resolution of the models themselves. Despite the drawbacks of remotely-sensed vegetation data, they have proven immensely useful in providing insight about the terrestrial biosphere due to their synoptic coverage and repeated temporal sampling [25, 34–37]. Furthermore, they

have a long data record and can provide context when analyzing phenology with new or different satellite products such as solar induced fluorescence (SIF), which is utilized in this study.

1.3 What is Solar Induced Fluorescence?

A fraction of photons incident on a leaf are absorbed by photosynthetic centers called chloroplasts. Once absorbed by chloroplasts, there are four main pathways that a photon can take: photosynthesis, constitutive thermal dissipation, nonphotochemical quenching (NPQ), and fluorescence [38]. Photosynthesis is the process in which leaves utilize the energy of photons in order to convert CO₂ and water into carbohydrates. Constitutive thermal dissipation and nonphotochemical quenching are both heat loss from the leaf, but the nonphotochemical quenching is an energy-dependent variable that is controlled by the mechanisms that regulate electron transport within the photosystems. The constitutive thermal dissipation, in contrast, is always present as heat loss from the leaf, even at night. Finally, solar induced fluorescence (SIF) are photons that are re-emitted by the plant photosystem at a slightly longer wavelength (lower energy level) and can be thought of as an inevitable leak during the photosynthetic process [38]. It is important to note that fluorescence is not a byproduct of photosynthesis, but a process that a photon may undergo instead of photosynthesis.

Recent developments in remote sensing allows us to measure SIF from space [39–41]. Observing direct radiative emissions of chloroplasts from space could provide a great deal of insight about how the terrestrial biosphere behaves by providing a constraint on regional scale photosynthesis (gross primary production, GPP). The amount of carbon assimilated by plants through photosynthesis is the largest carbon flux between the atmosphere and the terrestrial biosphere [42]. Therefore correctly estimating global and regional GPP is of the utmost importance in understanding the carbon cycle, its sources and sinks, and how it may respond to climate change. Large scale GPP (regional to global), which cannot be directly observed, has been estimated in the past using satellite products such as vegetation indices or canopy biophysical variables such as LAI or the fraction absorbed of photosynthetically active radiation (fPAR) [43–46]. None of these products,

however, are able to capture the highly variable nature of photosynthesis [47,48]. SIF, on the other hand, is intrinsically linked to photosynthesis through chloroplast mechanics. Research has shown a strong linear relationship between GPP and SIF using both gridded GPP products [40] and flux-tower GPP [49–51] (Figure 1.1), though the nuances of the SIF-GPP relationship still needs further exploration.

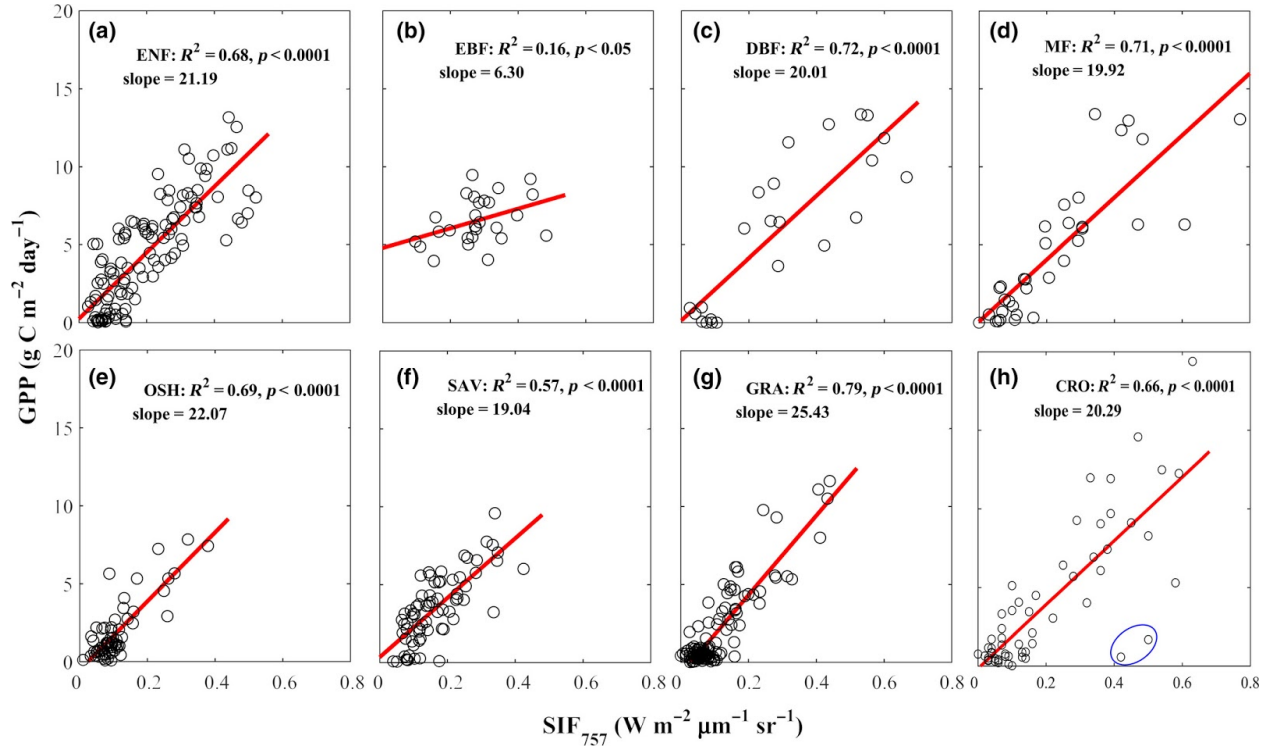


Figure 1.1: Scatter plots of daily Orbiting Carbon Observatory 2 (OCO-2) SIF retrievals and flux tower GPP from specific biomes. Each plot represents a difference biome: (a) evergreen needleleaf forests (ENF); (b) evergreen broadleaf forests (EBF); (c) deciduous broadleaf forests (DBF); (d) mixed forests (MF); (e) open shrublands (OSH); (f) savannas (SAV); (g) grasslands (GRA); (h) croplands (CRO). The red solid lines are fitted linear regressions lines. All biomes except evergreen broadleaf forests show good agreement. From Li et al. [51]

Furthermore, SIF retrievals are less biased by atmospheric scattering than vegetation indices. This is because SIF emissions happen to overlap with discrete bands of decreased solar intensity called solar fraunhofer lines. These dark lines in the solar spectra occur due to gases in the solar atmosphere that absorb photons within small ranges of wavelengths. Because there is no other known major source of photons within fraunhofer lines except plant fluorescence, satellite obser-

vations of photons in these bands must be coming directly from plants. Therefore, even though fluorescence photons are also scattered as they travel through the atmosphere, they come from a definitive source, which makes satellite SIF retrievals less biased by atmospheric scattering [52]. Satellite SIF observations are intrinsically at a pixel scale, which means that the satellite is retrieving the SIF photons emitted by within a large area of ground instead of the SIF emitted from a single plant or tree canopy. In order to compare leaf-level model predictions of SIF to satellite observations, appropriate scaling factors must be utilized to estimate a canopy level, and finally a landscape level SIF. These scaling factors are still being explored for a variety of vegetation structures [53]. Despite the caveats involved in SIF measurements, it is intrinsically linked to photosynthesis, and can provide information on the physiological behavior of ecosystems instead of a measure of its structure and greenness afforded by traditional vegetation indices [41]. SIF also has the potential to provide more information about vegetation in regions that have been historically difficult to observe due to cloud cover, dust, and other scattering phenomena.

1.4 Testing a terrestrial biosphere model

Our hypotheses about the primary drivers of the terrestrial biosphere and its phenology have been built in to the structure of the Simple Biosphere 4 (SiB4) model. This is a process driven model that uses a universal set of biological strategies to simulate the global terrestrial biosphere and a closed carbon cycle. Many terrestrial biosphere models (TBMs) use satellite data to prescribe their phenology while others use mechanistic approaches but require look-up tables in order to control growth and senescence [7]. The SiB4 model, however, introduces a process-driven dynamic phenology that does not rely on satellite or empirical data. Furthermore, the SiB4 model produces process-driven estimates of SIF. These attributes place the SiB4 model in a unique position to test our understanding of the primary drivers of phenology because its output can be compared directly to OCO-2 based SIF observations and MODIS-based LAI estimates. Therefore, the primary hypotheses that direct our research are as follows:

- SIF can be determined using absorbed solar radiation, photochemistry, and a canopy radiative transfer model.
- Phenology is a dynamic response of plants using a universal set of biological strategies that control allocation of carbon.

Chapter 2

Methods

2.1 The SiB4 model

At the time the first Simple Biosphere model (SiB1) was created, model simulated biosphere-atmosphere interactions were not biological process-based or self consistent. Thus, SiB1 was originally developed to simulate the actual physiology and morphology of vegetation structures and the resulting biophysical processes (i.e. fluxes of water, heat, and momentum) as part of global climate models. SiB1 was built to take into account how plants used biological strategies to efficiently use gas and water to maximize their growth and survival [54]. SiB2 was then built to incorporate a process-based photosynthesis model and simulate more realistic latent and sensible heat fluxes and carbon assimilation rates over large scales [55]. The photosynthesis model was based on enzyme kinetics described by Farquhar et al. [56] and is linked to the surface energy budget and the atmospheric climate through stomatal conductance [55,57–59]. Eventually SiB3 was created to include prognostic calculations of moisture, temperature, and trace gases in the canopy air space [60–62], improved hydrology, and improved photosynthesis [62–67]. Each version of SiB was developed to improve modeling capabilities and address specific concerns and uncertainties in the carbon cycle. SiB4 represents a significant step forward for the SiB suite of models by combining ideas from past versions of SiB, including those discussed above, and incorporating recent developments in terrestrial biosphere modeling [68]. SiB4 utilizes a new dynamic prognostic phenology scheme, carbon fluxes, and dynamic allocation to cascading carbon pools to create a predictive and self-consistent model of the terrestrial biosphere. The SiB4 model includes several new features that are described in detail in Haynes et al. [68], but we will provide a description of the fundamental model structure below.

The SiB4 model requires only three sets of inputs: meteorological data (for this study from MERRA-2), soil properties such as clay fraction and soil reflectance, and a map describing frac-

tional land cover. The soil properties are garnered from a variety of sources (see Haynes et al. [68] for details). SiB4 uses area mixtures of plant functional types (PFTs), rather than biomes, to describe global land cover because it reduces the complexity of representing heterogeneous plant types and can, instead, take advantage of leaf level eco-physiological functions to represent each specific plant type [69]. Each PFT (described in Table 2.1) is grouped by the plant type (forest, shrubs, or grasses), leaf type (broadleaf or needleleaf), and foliage type (deciduous or evergreen). Tundra environments tend to behave in unique ways, and thus have their own separate tundra grass and shrub PFTs. SiB4 uses a crop phenology model developed by Lokupitiya et al. [70], and only has explicit crop PFTs for maize, soybeans, and winter wheat. All other crops around the globe are not directly represented, but instead are grouped into either the generic C3 or C4 croplands PFT.

Table 2.1: Plant functional types that are input in to the SiB4 model.

Plant Functional Type	Abbreviation
Desert and Bare Ground	dbg
Evergreen Needleleaf Forest	enf
Deciduous Needleleaf Forest	dnf
Evergreen Broadleaf Forest	ebf
Deciduous Broadleaf Forest	dbf
Shrubs (non-Tundra)	shb
Tundra Shrubs	sha
Tundra Grassland	c3a
C3 Grassland	c3g
C4 Grassland	c4g
Generic C3 Crops	c3c
Generic C4 Crops	c4c
Maize	mze
Soybeans	soy
Winter Wheat	wwt

One of the most significant updates that distinguishes SiB4 from the past SiB versions, and from most other terrestrial biosphere models, is its dynamic prognostic phenology. SiB4's approach to simulating phenology was created to integrate two commonly used strategies: growing-

degree day approach (GDD) and growing season index (GSI). The growing degree day approach traditionally uses temperatures in order to time the shift between phenological stages. The growing season index approach uses thresholds of humidity, temperature, and light to predict the state of vegetation. By integrating ideas from both of these approaches, SiB4 utilizes simulated vegetation state and environmental factors (precipitation, day length, temperature, etc.) to shift plants through five stages of phenology: emergence, growth, maturity, senescence/stress, and dormancy. Phenological stages control the dynamic allocation of photosynthate to leaves, stems, root, and seeds throughout the season. Plants shift from maturity to senescence by predicting the most efficient use of the scarce resources available to the plant. Therefore, when projected respiration costs of the next increment of leaf area exceeds the amount of carbon likely to be fixed from that leaf, plants will start to shift their carbon allocation to roots and reproduction, triggering senescence. This dynamic strategy allows plants to move through phenological stages at vastly different rates. For example, arid environments may rapidly progress through all the stages when responding to acute rain events, while tropical forests may never reach a dormant stage. Furthermore this strategy allows each plant type, and plants at different latitudes, to have different responses to environmental factors.

SiB4 uses a system of first-order linear differential equations to control the flow of carbon between eleven carbon pools [71, 72]. There are five live carbon pools, composed of canopy and root structures, and six non-living carbon pools, composed of three above-ground pools of decaying biomass at varying rates, and three soil pools of varying decay rate. Carbon taken up during photosynthesis is allocated to the live carbon pools, and carbon in live pools are eventually transferred to the dead carbon pools. All pools release carbon through respiration.

SiB4 simulates a closed carbon cycle. Carbon allocation, storage, and turnover determine the above and below-ground biomass, which then feeds back on carbon assimilation and respiration. Every time step (10 minutes) SiB4 computes albedo, respiration, soil moisture, and temperature. It uses this information to compute moisture, carbon, and energy fluxes every time step. Once daily SiB4 takes into account disturbances from crop harvesting and livestock grazing. Then at

the end of each day it sums up the carbon fluxes and updates the carbon pools. Once the pools have been updated, the land surface properties are updated and used for the next day's rates of photosynthesis, carbon pool transfer, autotrophic and heterotrophic respiration. Carbon does not move laterally across grid boxes, except crop biomass, which is distributed to nearby population centers. This closes the carbon cycle in each gridcell, providing self consistent predictions of the state of vegetation, carbon assimilation rates, and land-atmosphere exchanges.

Using the strategies described above, SiB4 predicts a plethora of biological and physical variables in single, self-consistent, mathematical framework (see Figure 2.1). Of explicit importance to our analysis, SiB4 utilizes the live carbon pools to predict a daily LAI and predicts a process-driven leaf-level SIF [38]. The SIF predictions use a system that assigns rate coefficients to describe probabilities of the four pathways that a photon can take after being absorbed by a chloroplast (as listed in the introduction: photosynthesis, thermal dissipation, nonphotochemical quenching, and fluorescence). The probabilities are assumed to be mutually exclusive, the sum of which is unity. The amount of photons lost to thermal dissipation is dominant (95% or greater depending on the temperature). The proportion of photons that go to the other three pathways (photosynthesis, NPQ, and SIF) will change based on temperature, light, moisture, and the limitations of internal leaf structures. We used hourly output of modeled SIF from September 2014 to present (the same as the OCO-2 SIF record) and daily LAI estimates over the period 2000-2017.

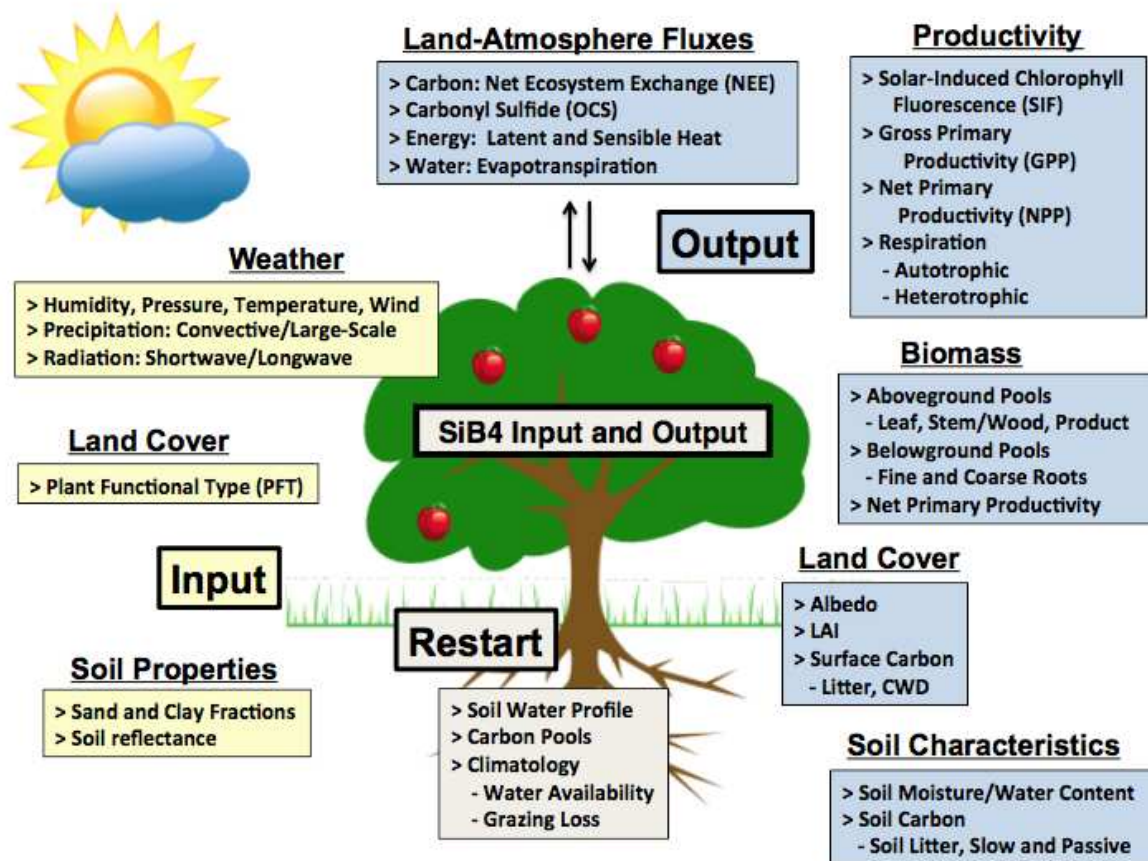


Figure 2.1: The SiB4 required inputs (yellow boxes), restart information (grey boxes) that are updated every time step, and the SiB4 output (blue boxes).

2.2 Observation datasets

We use observation datasets of LAI, NDVI, and SIF in order to analyze SiB4 phenology and improve our understanding of biome specific behaviors in the model. We use Terra MODIS LAI data from the National Aeronautics and Space Administration (NASA) Near Earth Observatory website (neo.sci.gsfc.nasa.gov). The data is received on a global 0.5x0.5 degree rectilinear grid and in 8-day composites, which are created using maximum value compositing [73]. Maximum value compositing, the process of choosing pixels with the highest value within each composite period, are used by the MODIS team in order to correct for low bias caused by atmospheric scattering

effects. In this case, the satellite pixels with the highest fPAR value every 8-days were selected, which dictated which LAI values were used. NASA warns that these data have been composited, scaled, and resampled to a coarse grid for visualization purposes, and should not be considered absolute values. We believe that these data are acceptable for our study, however, as we also would have composited the LAI data to a coarse grid in order to match the model resolution.

We use NDVI data over the years 2000-2017 from the NASA/GSFC Global Inventory Modeling and Mapping Studies (GIMMS) group [74]. The data was obtained as 15-day composites, which are made using maximum value compositing, on a fine grid (1/12 degree). We then composite the data to the same coarse grid (0.5x0.5 degree) as the model and MODIS LAI data using a bilinear interpolation scheme.

We obtain our fluorescence data from the Orbiting Carbon Observatory 2 (OCO-2). We use the daily post-processed SIF Lite files, which have been quality controlled to correct for altitude, outliers, scenes that are too bright or dark, high scattering, and clouds [40]. Each SIF retrieval in the Lite files has an associated biome classification based on the International Geosphere-Biosphere Programme (IGBP) land cover system (see Table 2.2). The OCO-2 satellite flies in a sun synchronous orbit, covering the same track every 16 days, always at approximately 1:30pm local time. The satellite swath is approximately 10km wide and consists of eight independent cross-track pixels, each with the footprint of 1.3 x 2.25 km. OCO-2 spectrometers take 24 spectra per second providing a high density of retrievals. The SIF retrievals from OCO-2 are taken in a spectral regime known as the O2-A band (757-775nm), which overlaps with the SIF emission spectrum (660-850nm) [75]. Because these spectra overlap with fraunhofer lines, the OCO-2 SIF retrievals are less affected by atmospheric scattering compared to traditional vegetation indices. This, combined with the small footprint of each pixel, allows the OCO-2 satellite to acquire SIF retrievals in regions that have historically poor data coverage, such as tropical rainforests. We use both vegetation indices and SIF products in this analysis, however, because they describe different aspects of vegetation (structure vs function), the MODIS data is widely used to describe phenology, and the

long data record of MODIS derived NDVI and LAI can provide context for the SIF comparisons, which is only 3 years (September 2014 onward).

Table 2.2: IGBP classifications of land cover.

Class	Description
0	Water
1	Evergreen Needleleaf Forest
2	Evergreen Broadleaf Forest
3	Deciduous Needleleaf Forest
4	Deciduous Broadleaf Forest
5	Mixed Forests
6	Closed Shrublands
7	Open Shrublands
8	Woody Savannas
9	Savannas
10	Grasslands
11	Permanent Wetlands
12	Croplands
13	Urban and Built-Up
14	Cropland/Natural Vegetation Mosaic
15	Snow and Ice
16	Barren and Sparsely Vegetated

OCO-2 retrievals include three different viewing angles from the satellite: directly overhead (nadir), from a shallow angle (glint), and focusing on a single point on the ground and tracking it by changing the viewing angle as the satellite flies overhead (target). These measurement modes are not directly comparable to each other because each has different biases. Only nadir mode SIF data was used for this analysis because it is much more abundant than target mode and has significant advantages compared to glint such as a higher spatial resolution, a greater signal-to-noise ratio over land, and has a higher chance of retrieving values over cloudy regions or areas of significant topography [75]. Furthermore, nadir follows a similar ground track each 16-day cycle, allowing it to better capture variability over time [75], which is crucial to our analysis of seasonality.

The OCO-2 SIF data is re-gridded in 2 different ways: to a 0.5x0.5 degree rectilinear grid over all of the biome types, yielding a total gridcell average; and to a 0.5x0.5 degree rectilinear grid with a gridcell average for each biome (IGBP). We use the biome-specific grid cell averages of satellite SIF to analyze the SiB4 PFT-specific SIF estimates from the canopy. We use the total gridcell average (over all biomes) to analyze phenology of the general region, as described in the phenology section of the methods below.

2.3 Model SIF scaling from canopy to the landscape

In order to analyze the scaling factors used to create canopy level SIF estimates in the SiB4 model, we compared SiB4 canopy-level SIF estimates from specific PFTs to OCO-2 SIF measurements from the most comparable biome type, as dictated by IGBP biome classification. The model SIF estimates were collocated to the nearest gridcell and hour as the observed SIF. We were not able to use the same biome map for the model as the Satellite because the PFT map in each 0.5 degree gridcell in SiB4 has a predefined fraction of each PFT but no information on how the PFTs are spatially arrayed. We removed biome-specific OCO-2 SIF gridcell averages that had less than 30 retrievals per day per gridcell. We also required that the gridcell had at least 20% areal fraction of the PFT being compared. This was done in an attempt to reduce errors due to model behavior for a PFT when it covered a very small fraction of the gridcell. Finally, the grassland comparisons were split up by latitude in an attempt to separate observed SIF values into C3 and C4 dominant signals because the IGBP land classification map does not distinguish between C3 and C4 grasses. The SIF observations over grasslands were compared to the modeled C4 grass SIF estimates in the tropics (15°S-15°N) and modeled C3 grass SIF estimates in the northern mid-latitudes (40°N-60°N).

2.4 Choosing geographic regions for analysis

We confined our analysis of phenology to specific regions around the world (Figure 2.2). These regions were chosen in order to display the behavior of certain types of ecosystem (e.g. grasslands, crops, evergreen needleleaf, etc.). Thus, many of these regions are dominated by a specific

PFT, or a specific group of PFTs. This was done in order to analyze how the phenological drivers of different PFTs in the model compare to the real world. Note that acronyms ENF and DBF on the map refer to evergreen needleleaf forests and deciduous broadleaf forests. Table 2.3 displays the percent areal coverage the PFTs for each region, which are based on the land cover map input to the SiB4 model for our analysis.

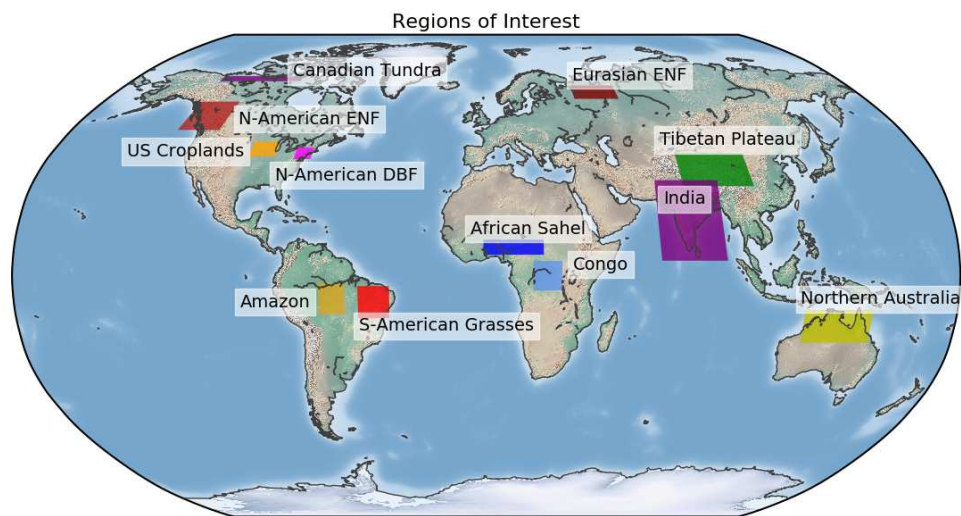


Figure 2.2: Map showing all of the regions used for phenological analysis.

Table 2.3: IGBP classifications of land cover.

Sites	1st most abundant	2nd most abundant	3rd most abundant
N-American ENF	38% enf	23% dbg	14% sha
US Croplands	45% mze	29% soy	8% dbf
N-American DBF	38% dbf	13% c3g	13% mze
Amazon	51% ebf	16% dbf	13% c4g
S-American Grassland	47% c4g	16% dbf	13% dbg
African Sahel Grassland	59% c4g	14% dbg	14% shb
Congo	60% ebf	13% c4g	12% shb
Eurasian ENF	51% enf	17% dbg	13% sha
Tibetan Plateau	71% dbg	19% c3a	3% c3g
India	32% c3c	27% dbg	8% wwt
Northern Australia	33% c4g	32% dbg	15% c3g

2.5 Determining the timing of phenological transitions

In order to analyze the phenology of the SiB4 model we gathered 8-day MODIS LAI, 8-day composited OCO-2 SIF, and 15-day composited GIMMs NDVI data over each specific region of interest and averaged them over the spatial dimension in order to create a time series. The OCO-2 SIF used in the phenology metrics were averaged over all biome types to get a total gridcell average. Each time series was gap-filled with linear interpolation to replace 8-day periods that had no data or were below a specified threshold for percent data coverage (1% for OCO-2 given the extremely small footprint and linear nature of the narrow satellite tracks, and 30% for LAI and NDVI). Then the MODIS LAI and OCO-2 SIF 8-day data were smoothed backward and forward by a 40 day (1-1-2-1-1 window) moving average.

The NDVI 15-day composites were smoothed back and forward by a 45 day (1-2-1 window) moving average. These datasets were smoothed in such a way in order to create idealized curves that do not change the general shape of the seasonal cycles, but also allow for the intercomparison of datasets with different temporal resolutions. Therefore the smoothed curves are meant to be representative of the general seasonality of the region, based on the variable that is represented in

each dataset (LAI, NDVI, SIF, etc.). The smoothed time-series were then interpolated to a daily temporal resolution in order to record timing of phenological transitions. It should be noted that the level of interpolation and smoothing makes it difficult to record the exact date of phenological transitions [76] but for this analysis we are more interested in the relative differences between observation datasets and the model output than the exact date of each phenological transition.

We compared the observation datasets to SiB4 model output of SIF and LAI over the same regions. In this case the model output was not collocated to the nearest gridcell, but instead shown in its entirety over the region. Only SiB4 SIF output from 1:30 pm local time was used, which is approximately the same time as the OCO-2 pass-over time. The model LAI and SIF output were composited to the same 8-day resolution as the corresponding observation data sets, and then processed using the same steps, except the gap-filling, used for the observed data as described above. Since SiB4 does not predict NDVI explicitly, we did not compare the two directly, but we decided to include NDVI in our analysis of phenology because it is widely used to estimate phenology.

The phenology of these datasets were then analyzed by splitting the data up in to individual phenological years, where a phenological year was defined as a year long period from beginning to end of each growing season. The start of each phenological year was chosen to be in the middle of a period of minimal vegetation function or canopy structure, such as the winter or a dry season. Then each seasonal cycle was normalized using a ratio based on White et al. [77] where X is a time series of a variable in a given region:

$$\frac{X - X_{\min}}{X_{\max} - X_{\min}} \quad (2.1)$$

The ratio was applied to the time series of each phenological year of all observed and modeled variables in each region. The ratio was applied to each year in order to normalize the ratio by the maximum and minimum value of each growing season. Some years were not used if they were found to have too many significant gaps in the data: there must be data in the original time series within 60 days of the beginning or end of each phenological year; at least 35 composited

8-day periods of LAI data within the phenological year; at least 14 composited 15-day periods of NDVI data within the phenological year; and at least 25 composited 8-day periods of SIF data. We decided that we required fewer 8-day periods of SIF data within each year than LAI data because the gaps in the SIF record tended to be more dispersed throughout the year, while LAI data gaps tended to be more concentrated making a reasonable estimate of phenological transitions difficult. These requirements were utilized so that we could ensure that a full seasonal cycle was used when determining the timing of phenological transitions.

By normalizing each regional time series using the ratio above we were able to compare the apparent phenological transitions of each dataset. We defined the start of season (SOS) and end of season (EOS) as the first and last day of the phenological year that the ratios crossed a 25% threshold. We defined the start of maturity (SOM) and end of maturity (EOM) as the first and last day that the ratios crossed a 75% threshold. Figure 2.3 shows a flow-chart describing how the phenology was determined. We also compare the relative magnitudes of modeled and observed variables by plotting the average growing season in the original units instead of the as ratios.

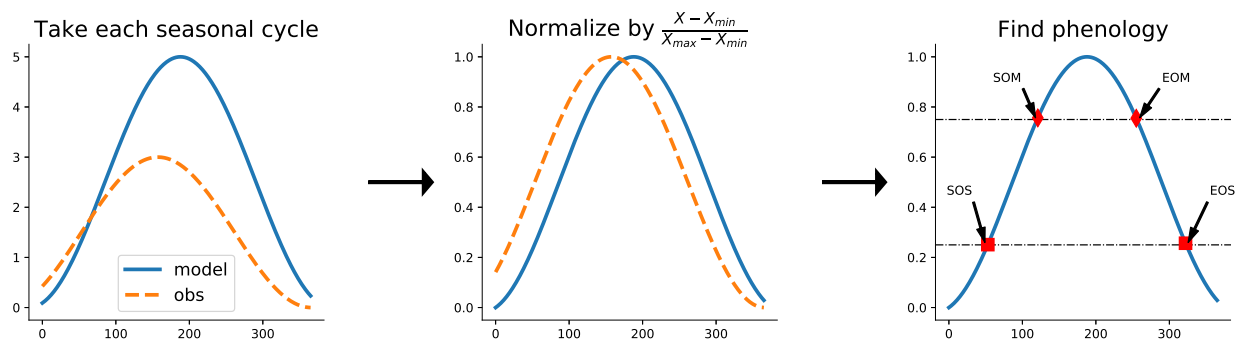


Figure 2.3: Flow-chart describing our phenology analysis. The first step is to split the time series of each variable of each region into individual seasonal cycles (left hand plot). The second step is to normalize each variable's seasonal cycle by the ratio shown above (middle plot). The final step is to determine the start and end of season (SOS and EOS) by identifying the first and last day that the 25% threshold is crossed, and the start and end of maturity (SOM and EOM) by identifying the first and last day that the 75% threshold is crossed.

Chapter 3

Results

3.1 SIF pixel-scale analysis

We compared modeled canopy SIF from specific plant types to satellite pixel SIF observations over the most comparable biome type from all over the globe (Figure 3.1). We find that the model consistently overestimates SIF for almost all plant types throughout the year compared to satellite observations. The magnitude of the overestimation, however, appears to be seasonally dependent. We are able to infer information about the seasonality of the model overestimation because the points are color-coded based on whether the model value was within six months before (labeled as growth on the colorbar) or within six months after (labeled as senescence on the colorbar) the peak month of SIF for that model gridcell. Therefore the dark blue or dark red points are generally observations found in the winter (or the dry season in some environments). In order to describe how to interpret the color coding of these plots, we will focus on SIF comparisons for deciduous needleleaf forests (Figure 3.1c), which displays a clear seasonal dependence. The winter model-observation ratios are clustered near zero (blue). When the model grows leaves and starts to photosynthesize (thus also simulating fluorescence) during the spring months, the model SIF compares well to the observed SIF, indicated by the blue-green dots that are close to the one-to-one line (thin black line). Then as the season shifts from spring to summer (shift from green to yellow dots) the average model SIF is well above the one-to-one line, which indicates that the model canopy SIF is overestimating the averaged SIF observations. Finally as the season shifts from summer to fall and then to winter (shift from yellow to orange and red) the overestimation is even greater, which indicates that not only is the model overestimating SIF, but it also has phenological differences with the real world over deciduous needleleaf forests. We can infer this because the SIF overestimation gets larger later in the season, indicating that the plants are greener in the model than the real world later in the season.

SIF comparisons over evergreen needleleaf forests (Figure 3.1a) also display a seasonal dependence, but the relationship differs from deciduous needleleaf forests. The model-observation ratios are clustered during the winter (blue and dark red) and summer (yellow) months but displays more variability in the spring and fall. This is indicated by the large standard deviations in the model bin averages (red dots and red error bars) over the low to mid range observations. Evergreen needleleaf comparisons also display the highest model overestimations during both spring and fall, which indicate phenological differences between model and observed SIF during both the transition into and out of maturity. Modeled evergreen needleleaf forests canopy rarely reach zero SIF creating an especially high bias during the winter compared to other PFTs. Modeled evergreen needleleaf SIF estimates also have the highest bias in general throughout the year compared to other plant types.

No apparent relationship exists between modeled and observed evergreen broadleaf (Figure 3.1b), which is indicated by the near constant bin averages of the modeled SIF across all observed SIF values and all times of year. Modeled SIF from deciduous broadleaf forests (Figure 3.1d) is the most accurately simulated compared to the satellite observations, averaging nearest to a linear relationship than any other plant type. The seasonal dependence of the model-observation relationship is less clear over deciduous broadleaf, but the model appears to slightly overestimate SIF during the spring and fall and slightly underestimate SIF during the summer, when compared to high SIF observation values. The tendency for the model to underestimate SIF at high values seems to be common to many of the PFTs, but many of the other PFTs only have a few points below the one-to-one line compared to the deciduous broadleaf forest. Modeled SIF estimates from the shrublands PFT are compared to the observed SIF over the open shrublands biome (Figure 3.1e). The modeled and observed SIF for shrublands have no apparent seasonal dependence and a highly variable relationship, which is indicated by the large standard deviations around the purple bin averages. The SIF comparisons for C3 grasses in the northern mid-latitudes and C4 grasses in the tropics indicate that the model overestimates SIF from grasses throughout all seasons on average, despite the few points that show a model underestimation when observed SIF is very high. As we will discuss further in the conclusions section, we do not know whether this overestimation is due

to the model SIF parameterizations, biases in the model photosynthesis mechanisms, atmospheric scattering effects in the satellite retrievals, or land heterogeneity in the satellite pixels.

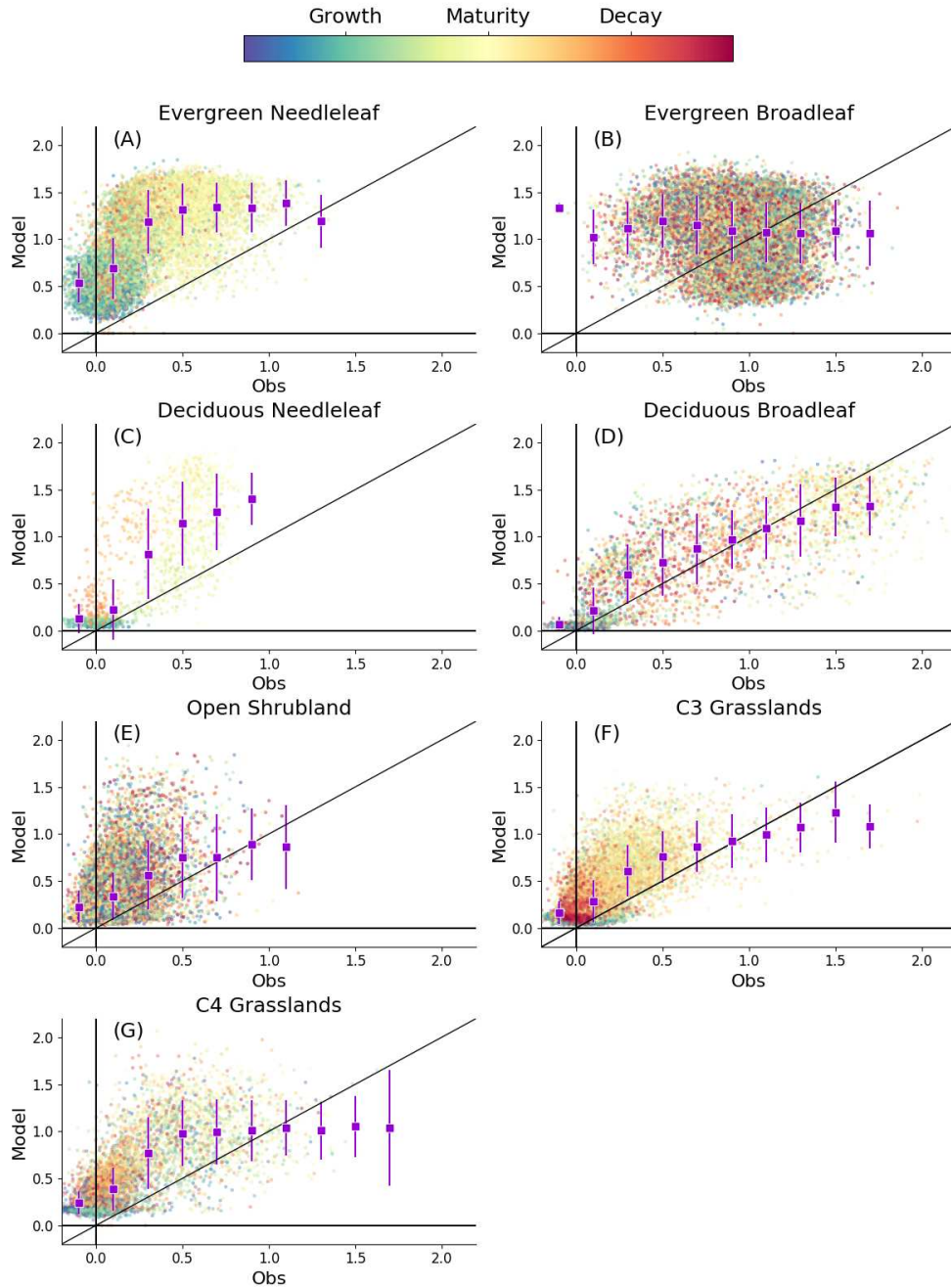


Figure 3.1: A comparison of SiB4 PFT-specific estimates of SIF from the vegetation canopy and satellite observed SIF over the most comparable biome type dictated by IGBP classification. Each point represents the average of at least 30 SIF observations from the specified biome type over a 0.5x0.5 degree gridcell within a given hour long period and the model estimate of SIF over the same PFT in the same gridcell and nearest hour. The points are color coded based on the time before or after the peak mode SIF of the gridcell the point was in. For example, if a point is dark blue, than it was around 5 months before the month of peak SIF in the model for that gridcell. The purple squares represent the average model SIF estimate for a 0.2 bin width of observed values. The purple error bars represent one standard deviation from the average. Plot F is a comparison of simulated C4 grassland SIF and observed SIF over tropical regions (15°S-15°N) and plot G is a comparison of simulated C3 grassland SIF over the northern mid-latitudes (40°N-60°N).

3.2 Phenology

3.2.1 Deciduous broadleaf forests

We compared the timing of phenological transitions as well as the average seasonal cycles of modeled and observed products over each region shown in Figure 2.2. It is important to note that, unlike the SIF scaling analysis, the remaining analyses compare modeled gridcell total SIF estimates (i.e. the sum of area weighted SIF estimates from each plant functional type each gridcell) to aggregated SIF observations over all biome types in the region. The model was most accurate in simulating phenology, canopy structure, and fluorescence in northeastern United States (Figure 3.2), which is dominated by deciduous broadleaf forests. The upper left plot of Figure 3.2 shows the average seasonal cycle of modeled and observed LAI over this region. The lower left plot shows the average seasonal cycle of modeled and observed SIF. The thin grey lines on both of the left-hand plots are the individual seasonal cycles of the observed data that make up the average observed season. The x-axes of the left-hand plots are day of year (DOY). Note that the DOY for all plots is not necessarily day of calendar year, but instead should be considered day of phenological year, which starts and ends where vegetation productivity is at its minimum for the region (i.e. in the winter in the northern latitudes, the dry season in the tropics, etc.). Both observed LAI and SIF are larger during the peak of the season, indicating that the model may be simulating a less dense canopy than the real world, which may be the reason the SIF is also underpredicting for the region.

The upper right-hand plot of Figure 3.2 shows the day of year (DOY) where the ratios of each seasonal cycle cross the 25% threshold (see flowchart of Figure 2.3). Therefore, on the upper-right hand plot of Figure 3.2, there are two lines for each data product: one lower on the y-axis showing the start of season (SOS) for each year; and another near the top of the y-axis showing the end of season (EOS) for each year. In contrast, the lower right-hand plot is showing the first and last day that the same ratios are crossing the 75% threshold each year, which is how we indicate the start and end of maturity (SOM and EOM, respectively). When comparing to MODIS LAI start of season, we find the model canopy greens up later, indicated by a model SOS that averaged 20 days later than observed. The 2 years of satellite SIF data indicate, however, that modeled fluorescence

began ramping up within 10 days of the observed fluorescence. This, may indicate that once SiB4 produces it's initial leaves and photosynthesis begins to increase, it may be taking too long to produce new leaves. Despite a late SOS, the model accurately predicts the timing of senescence, averaging only 2 days late compared to MODIS LAI, and 7 days late compared to OCO-2 SIF. The NDVI, in contrast, indicates a much longer season than both LAI and SIF observations (right-hand plots of Figure 3.2) averaging a start and end of season around 37 days early and 46 days late, respectively, compared to MODIS LAI. This region shows very little interannual variability in the growing season length. More analysis is needed to show that the model accurately predicts deciduous broadleaf forests in other climates, as this analysis was restricted to a small area of Eastern North America alone.

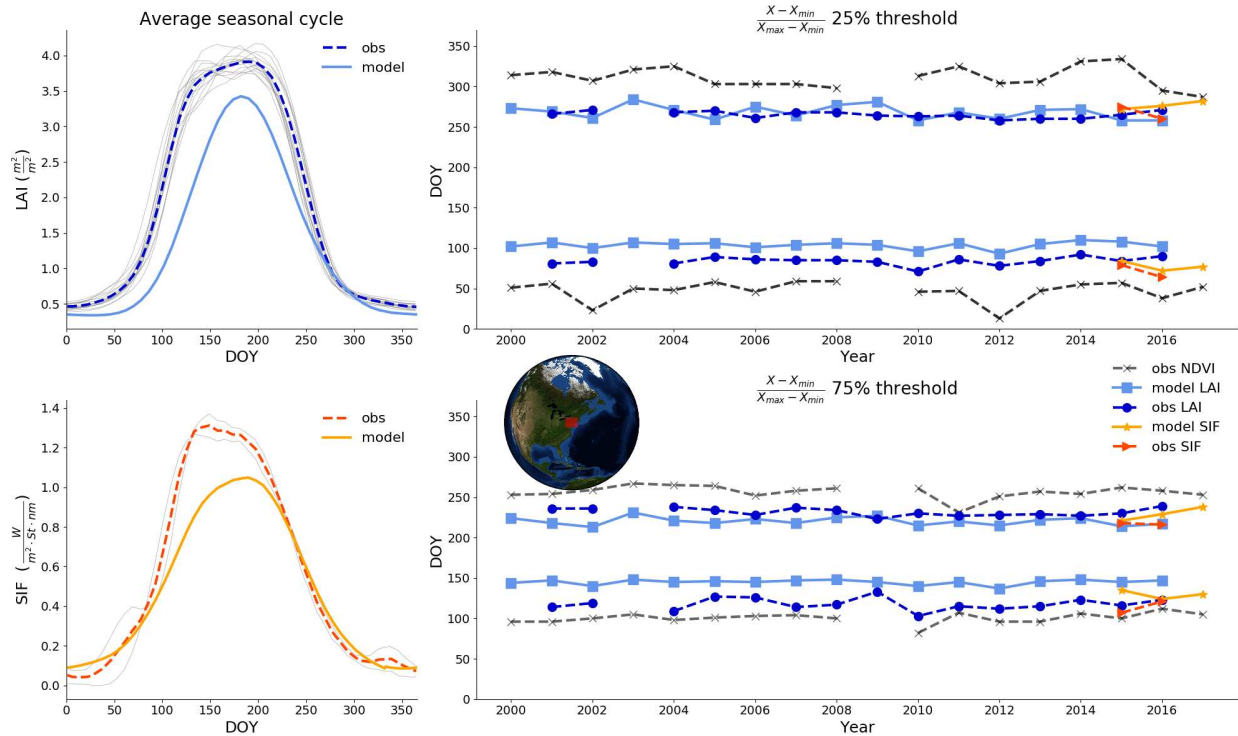


Figure 3.2: The figure above compares modeled and observed productivity and phenology over the north-eastern United States, which is dominated by deciduous broadleaf forests. The x-axes of the left-hand plots show the day of phenological year (DOY; which here is day since the latest period of minimal vegetation activity) instead of the day of the calendar year. The upper left-hand plot is the average seasonal cycle of modeled and observed LAI. The lower left-hand plot shows the average seasonal cycle of modeled and observed SIF. The upper right plot shows the first and last day of each growing season that the ratio of each time series crossed a 25% threshold. The first day this occurred each growing season was defined as the start of season (SOS) and the last day was defined as the end of season (EOS). The lower right plot shows when the ratios cross a 75% threshold, which was defined as the start and end of maturity (SOM and EOM). Note that the SIF record is only 2-3 years long. Please note that the colors remain consistent for each data product.

3.2.2 Tropical and sub-tropical grasslands

The SiB4 model simulates the growing season onset well in tropical and subtropical grasslands around the world, but tends to shift from maturity to senescence later than the observed from MODIS and OCO-2 (Figures 3.3-3.5). We find that over a grassland-dominant region of South American (Figure 3.3), LAI observations are consistently higher than modeled LAI (upper left-hand plot) while the SIF observations are higher during spring onset and maturity but not during

senescence (lower left-hand plot). When comparing modeled and observed LAI seasonality (upper right panel of Figure 3.3) SiB4 simulates an SOS that is generally within 10 days of observed values, but senescence is an average of 18 days late. According to the SIF comparisons, the model is late both in the SOS (19 days) and an EOS (39 days). Both in the SIF and LAI, not only does the end of season occur later in the model but so does the shift from maturity to senescence, averaging an EOM 16 days later in model LAI and 31 days later in model SIF.

We find similar phenological behaviors over northern Australia (Figure 3.4), which is composed of C4 grasses primarily, and C3 grasses and shrublands to a lesser degree. One difference between the South American region and Australia is that modeled LAI and SIF are both consistently higher than observations, except during the winter where model leaf area is generally lower than MODIS LAI (left-hand plots of Figure 3.4). The SOS and EOS comparisons in this region are similar to other grasslands regions because SiB4 simulates spring onset relatively well but has a senescence period that is significantly longer than remotely sensed vegetation data indicates. The SiB4 SOS averages 17 days early compared to MODIS LAI, and 21 days late compared to OCO-2 SIF. The model simulates a much longer growing season, however, because modeled LAI EOS averaged 69 days later than observed, and modeled SIF averaged 78 days later than observed. The model also tends to have a longer period of plant maturity over this region simulating an SOM 19 days early on average and an EOM delayed by 13 days. Similar to the NDVI seasonality over deciduous broadleaf, the NDVI over this region suggests a longer season than both observed LAI and SIF, averaging an EOS that is delayed by 51 days compared to MODIS LAI. The NDVI does agree well with MODIS LAI in the timing of the spring onset, however. There is some interannual variability in this region, but the discrepancies between modeled and observed phenology remain consistent, excluding LAI EOS in 2005.

The African Sahel is a crucial region in carbon cycle research, holding one of the worlds largest grasslands, and is poorly constrained by observations and in situ data [78]. We find, using both LAI and SIF observations, that the model simulates the spring onset relatively well in this region but simulates a senescence period that is too long and too slow (Figure 3.5). The model SOS is

an average of 9 days late compared to MODIS LAI and 15 days late compared to the OCO-2 SIF. Similar to other grassland regions, SiB4 simulated a far longer period of maturity and senescence, averaging 50 days late compared to MODIS LAI and 66 days late compared to OCO-2 SIF. The model SIF clearly has a dual peak pattern, due to the two distinct wet seasons of the Sahel region, but the observed SIF did not. Further investigation is needed to see if this is also a pattern in SiB4 photosynthesis or only in the fluorescence estimations. If the model photosynthesis does not show this dual peak pattern, then we may infer that the dual peak pattern shown in Figure 3.5 is due to the light availability before and after the wet season. The model also simulates a longer period of plant maturity than the observations (lower right panel of Figure 3.5).

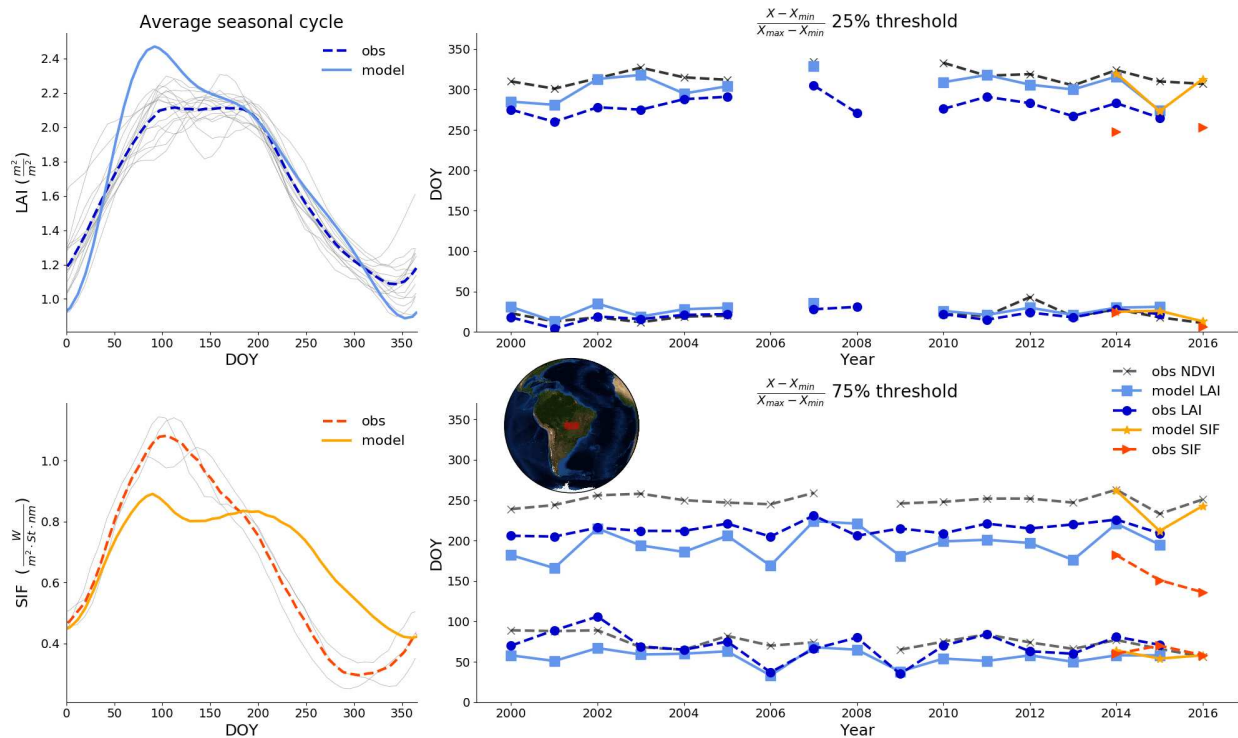


Figure 3.3: The figure above compares modeled and observed phenology and productivity, as described in Figure 3.2, over a region of South America dominated by C4 grasslands.

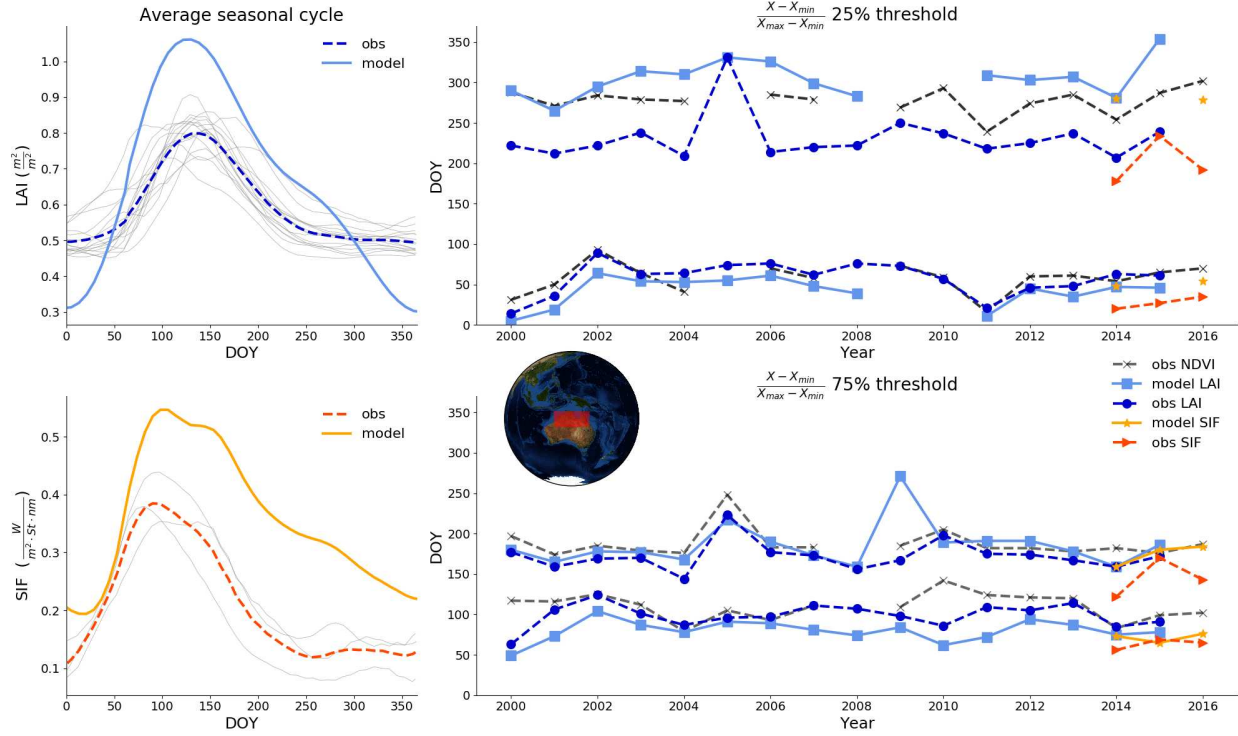


Figure 3.4: The figure above compares modeled and observed productivity and phenology, as described in Figure 3.2, over Northern Australia, which is dominated by C3 grasses, C4 grasses, and shrublands.

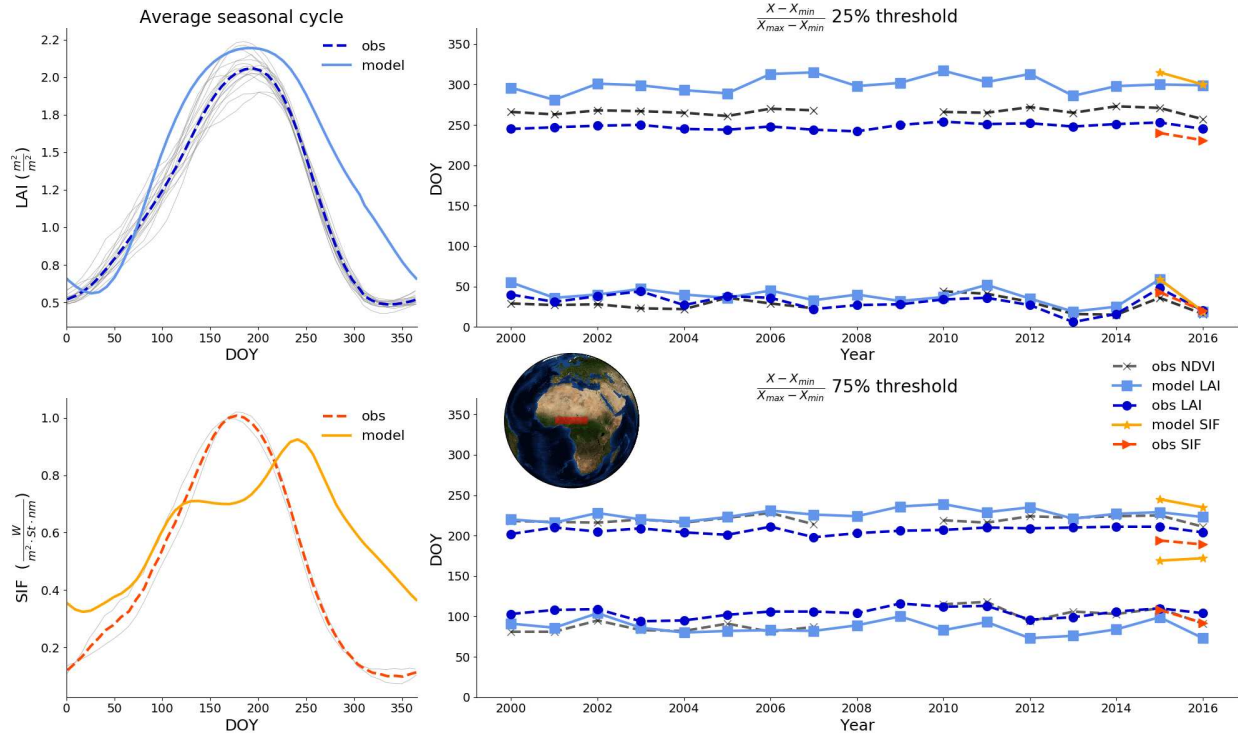


Figure 3.5: The figure above compares modeled and observed productivity and phenology, as described in Figure 3.2, over the African Sahel, which consists largely of a combination of C3 grasses, C4 grasses, and shrublands.

3.2.3 Agricultural regions

The model is able to reasonably predict the timing of cropland harvest in agricultural regions of the United States, but poorly represents either cropland planting dates or the timing of crop growth. SiB4 also tends to misrepresent crop phenology in other regions around the world. The United States corn belt is a region of industrial croplands in Iowa and the surrounding states. The primary crops in the region are corn, soybeans, and wheat. The model simulates each of these primary crops, and groups any other crops in to separate PFTs called generic C3 crops and generic C4 crops. Our analysis of the climatology and phenology of US agricultural land, often called the Corn Belt, (Figure 3.6) revealed that the model simulated too short of a growing season compared to observations, due to a green up that occurred too late. The model SOS was an average of 39 days late compared to observed LAI and 29 days late compared to observed SIF (upper

right-hand plot). The model was able to accurately capture the harvesting dates of crops in this region, however, averaging only 6 days later compared to observed LAI and 15 days compared to observed SIF. Interestingly, the model LAI consistently overestimated the leaf area magnitude during the summer in this region (upper left-hand plot) but underestimated SIF magnitude (lower left-hand plot). Similar to deciduous broadleaf and some grassland regions, the NDVI seasonality indicates a much longer growing season than the observed LAI and SIF in this region, averaging an SOS 33 days early and an EOS 44 days late compared to MODIS LAI.

We also compare the modeled LAI and SIF to observations over India (Figure 3.7), which revealed an interesting discrepancy between the generic cropland PFTs in the model and how crops are planted and harvested in the real world. Unlike grassland regions, the modeled croplands seasonality in this region are essentially phase shifted earlier in the year, thus missing both the spring onset and the senescence of vegetation. The model SOS occurs much earlier than both observed LAI (72 days early) and observed SIF (55 days early) consistently throughout the data record. The model EOS was also earlier than the corresponding observations but the magnitude of lateness was also more variable than the discrepancies seen in the SOS comparisons. This may be due to the dual peak pattern seen in the observations over this region, which could lead to a prolonged season depending on the magnitude and timing of growth. The modeled vegetation also reached the end of maturity, thus starting to senesce, earlier than observed, and sometimes even before observed SIF and LAI reached maturity (lower right-hand plot).

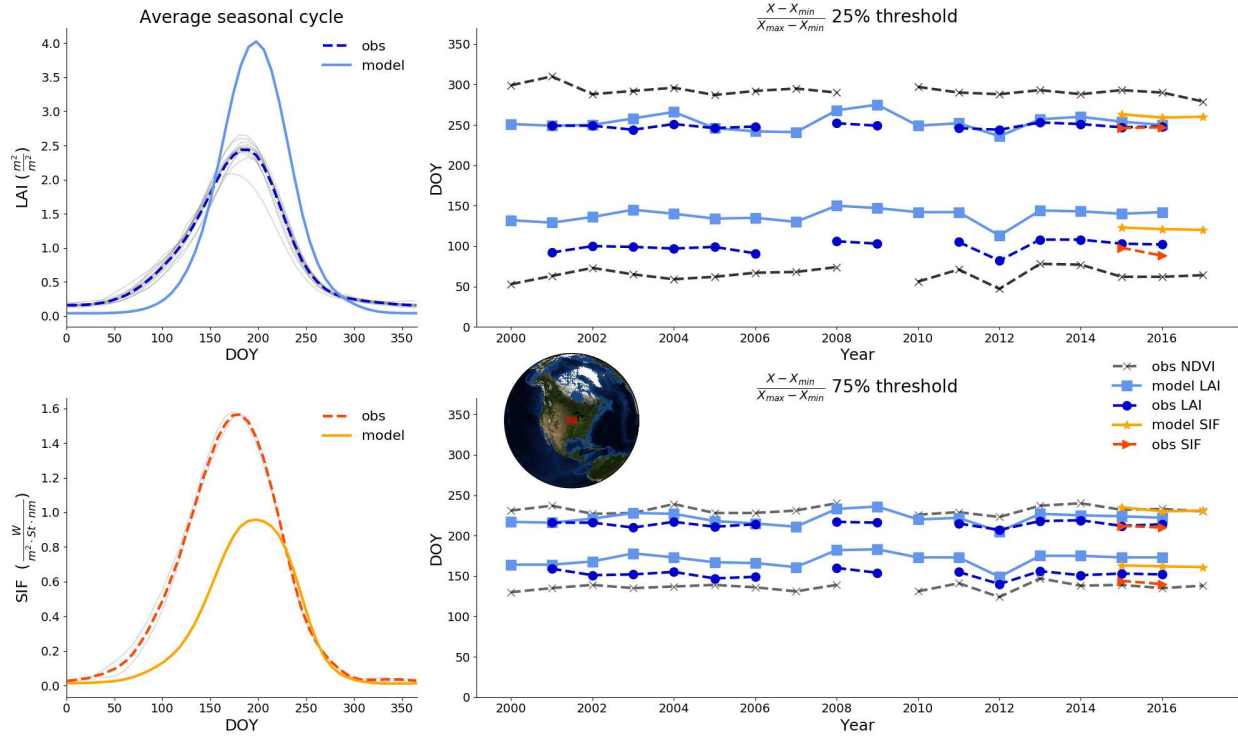


Figure 3.6: The figure above compares modeled and observed productivity and phenology, as described in Figure 3.2, over the Corn Belt of the United States, which is dominated by industrial crops such as corn and soybeans.

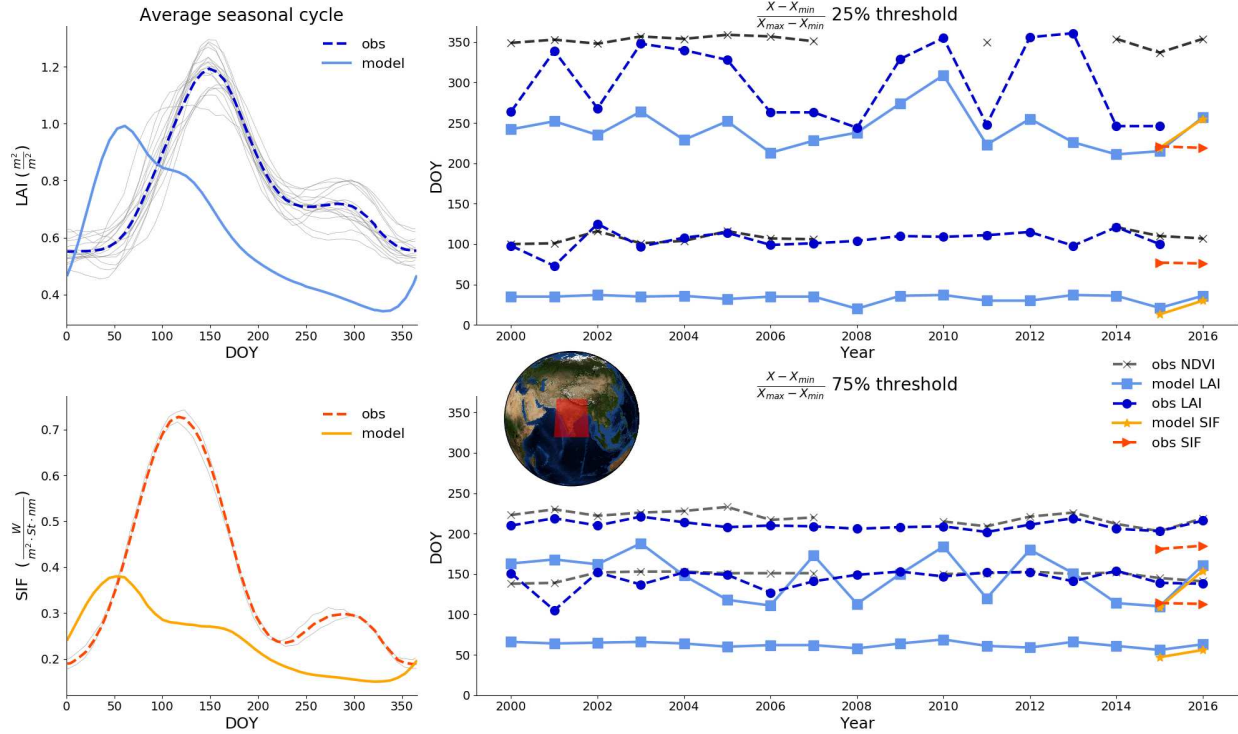


Figure 3.7: The figure above compares modeled and observed productivity and phenology, as described in Figure 3.2, over India, which has a large proportion of C3 croplands (32%, see in Table 2.3) and a mixture of small fractions of other PFTs. The model peaks that are seen are due to PFT contributions from C3 and C4 croplands.

3.2.4 Tibetan Plateau

We compare phenology and productivity of modeled and observed vegetation over the Tibetan Plateau (Figure 3.8). Also known in China as the Qinghai-Tibetan Plateau, this region is one of the most sensitive to climate change [79–81]. This region has experienced rapidly increasing temperatures as well as accelerated permafrost thaw in the past few decades [82], resulting in plant phenology shifts [80, 83]. These traits make this region ideal for studying plant phenology [84]. It should be noted that we do not analyze how the phenology in this region changes over multiple decades, but instead focus on the intercomparisons of phenology between different satellite products and the SiB4 model. We find that the model LAI is always lower than observed LAI while model SIF is consistently higher than observed, though both LAI and SIF in this region are very

small in general (left-hand plots). When comparing modeled and observed LAI, SiB4 seems to simulate green up very well in this region, averaging only 6 days earlier than observed. According to the LAI comparison, SiB4 does have a slower rate of senescence, however, because the EOS is 19 days later than observed while the EOM is only 7 days late on average. The model SIF is not only greater than observed, but also tends to have a broader season, averaging an SOS and EOS that are 33 days early and 29 days late, respectively. It should be noted that the observed SIF averages below zero during the winter, which are non-physical values for SIF. This may be noise in the data or due to offset corrections in the retrieval.

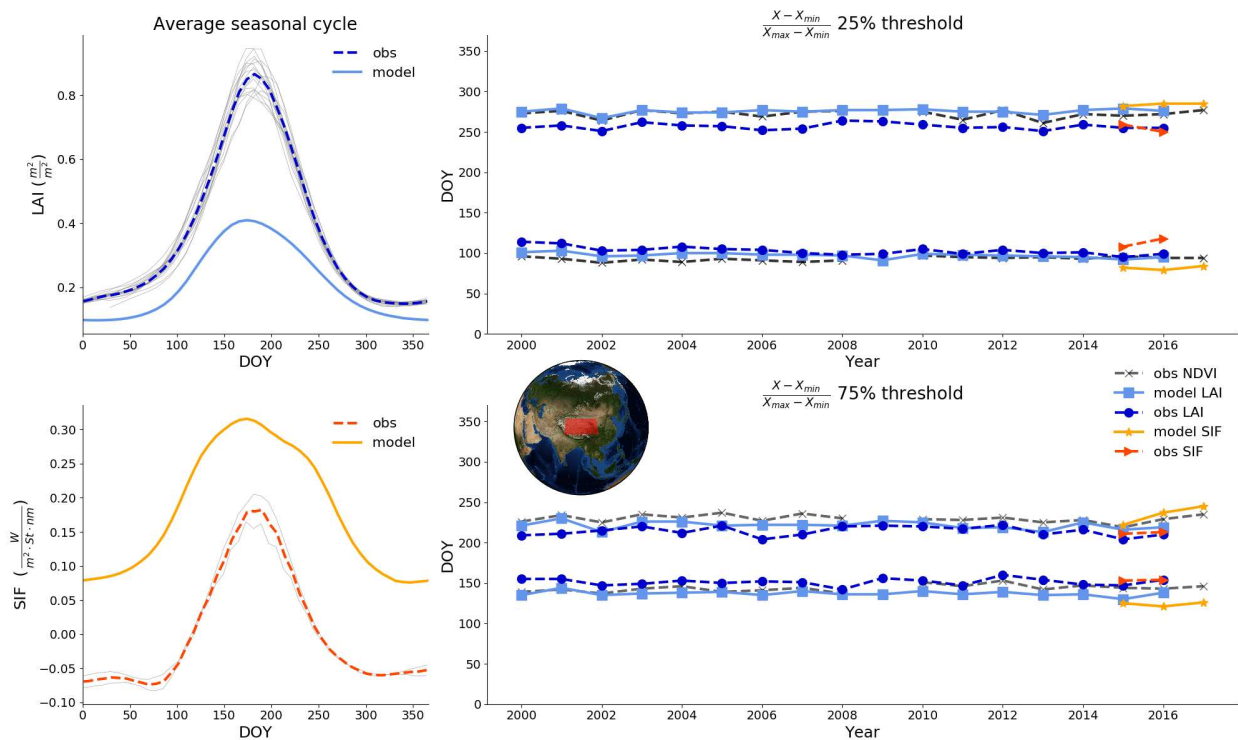


Figure 3.8: The figure above compares modeled and observed productivity and phenology, as described in Figure 3.2, over the Tibetan Plateau, which consists largely of tundra C3 grasslands.

3.2.5 Boreal forests and grasslands

For high latitude environments, we are unable to complete a phenology analysis due to gaps in the MODIS LAI and OCO-2 SIF data record caused by a lack of sufficient light in these regions during the winter months. We do compare the average seasonal cycles of observed and modeled SIF, however (Figure 3.9). We find in all boreal environments compared, whether dominated by tundra grasses or evergreen needleleaf forests, that SiB4 consistently overpredicts SIF. This is consistent with the overpredictions of canopy SIF from evergreen needleleaf forests (see Figure 3.1).

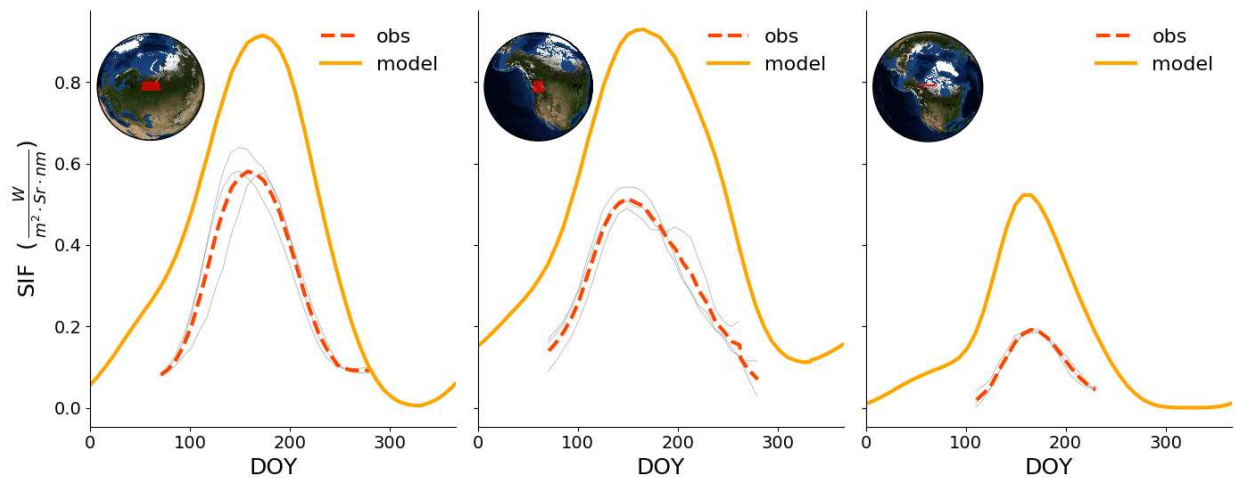


Figure 3.9: SIF comparisons of modeled (solid line) and observed data (dashed line) over Eurasian evergreen needleleaf forests (left-hand plot), North American evergreen needleleaf forests (middle plot), and Canadian tundra (right-hand plot). The Canadian tundra vegetation is largely composed of tundra C3 grasses.

3.2.6 Evergreen broadleaf forests

Tropical rainforests, especially those in Africa, are poorly constrained by in situ observations due to political instability and lack of infrastructure necessary to facilitate research [85]. Satellite observations over rainforests are often attenuated by heavy cloud cover. Although rainforests do exhibit some seasonality, which is possibly driven by light availability [86], we were not able

to identify stark seasonal cycles. Therefore, we did not complete phenological analyses in these regions. We also do not show a comparison of the average year of modeled and observed LAI due to significant gaps in the LAI coverage. We do compare modeled and observed SIF, however, over the Amazonian and Congolese Rainforest (Figure 3.10). The model was able to accurately capture the relative aseasonality of regional photosynthesis in both the Congo and the Amazon. There also appears to be an anti-correlation between modeled and observed SIF. This may be due to differences in weather in the MERRA-2 and the real world, where SiB4 is predicting SIF for cloudy scenes, while the observed values, by nature of the satellite retrievals, only represent sunny to moderately cloudy scenes.

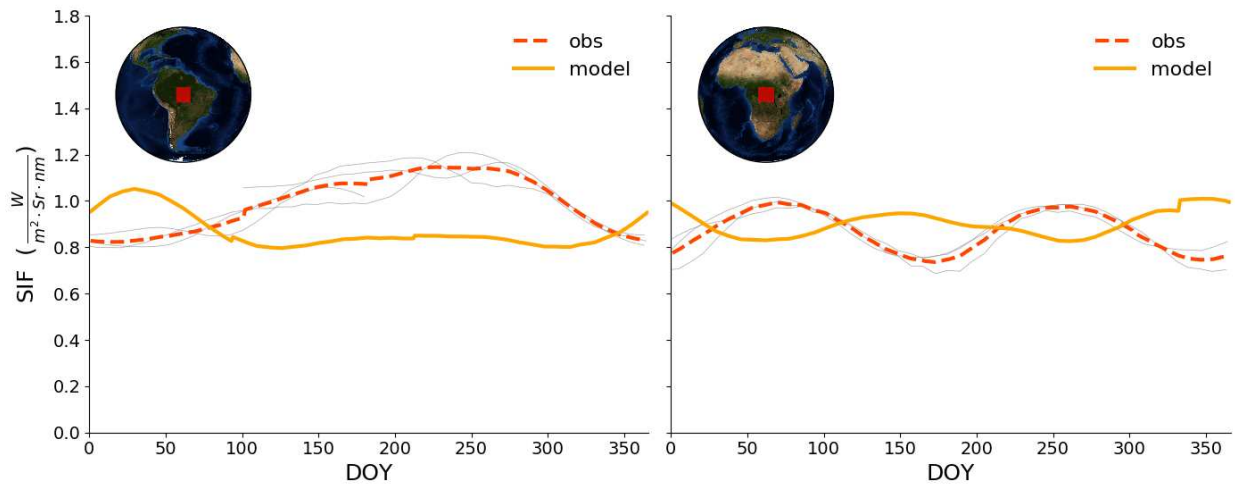


Figure 3.10: SIF comparisons of modeled (solid line) and observed data (dashed line) over Amazonian (left-hand plot) and Congolese (right-hand plot) evergreen broadleaf forests.

Chapter 4

Discussion and Conclusions

The SiB4 model is unique both in its ability to estimate SIF using enzyme kinetics and photochemistry and in its process-driven strategy to dynamically shift global vegetation through phenological stages. We tested the model's ability to predict SIF for varying plant types (Table 2.1) by comparing modeled canopy estimates of SIF to aggregated satellite pixels of SIF. We found that, for a majority of observed pixels, the modeled canopy SIF is consistently higher than the observed SIF values across all plant types and climates, with the exception of deciduous broadleaf forests. There are many possible reasons that the SiB4 canopy SIF estimates were higher than pixel-scale SIF observations, primary of those being that the satellite is observing fluorescence over heterogeneous pixel instead of a homogeneous canopy. Heterogeneity in the satellite pixel will include bare ground, other plant types, water, and other artifacts, that would cause SIF emissions from the pixel to be lower than if the pixel was only composed of a homogenous plant canopy. Therefore, the modeled SIF estimates from each PFT, which assumes a homogenous canopy, may be correctly simulating the average canopy but it is difficult to verify with aggregated satellite pixels. This would also imply a relationship between the overestimation of pixel-scale SIF and the density of the canopy that is being observed, which warrants further research. Deciduous broadleaf, for example, tends to form dense canopies in the real world allowing satellites to see a more homogeneous scene, and it is the plant type where observed and modeled SIF compare best.

Another component that could contribute to the high modeled SIF emissions is the canopy scaling factor that is used in the model to scale SIF from a single leaf to an entire plant canopy. The scaling factors used in the model are empirically estimated using a canopy radiative transfer model that splits the canopy into layers, estimates the amount of photons emitted by each layer, models the recapturing of fluorescence photons by other parts of the canopy, and estimates the total amount of fluorescence that escapes the canopy back into the atmosphere. Due to the especially high bias in evergreen needleleaf forests, the scaling factor used in these environments may be over

predicting the amount of photons that are allowed to escape the canopy. Snow cover in satellite pixels may also dampen the SIF signal from evergreen needleleaf forests. The model, however, does not take this into account, which could be causing the especially high overestimation in the winter for this biome.

One final component that may explain the model overestimation of SIF is that the model does not take in to account atmospheric scattering of fluorescence photons that occur between the canopy and the satellite. Atmospheric scattering can reduce the SIF signal by approximately 20% with cloud optical thicknesses around 2-5 [52], though this would not explain all of the model overestimation. These results emphasize the need for more ground-based canopy estimates of SIF over a variety of plant types.

Despite the mismatch between modeled canopy estimates and satellite observations we learned several interesting facts about about how SiB4 modeled SIF compares to the real world. For example, comparing the average seasonal cycle of landscape scale model estimates of SIF (i.e. gridcell averages of regions) showed that the model simulates seasonal cycles of fluorescence of a reasonable magnitude in many environments.

When comparing remotely sensed phenology, we found a common pattern in many parts of the world: AVHRR-based NDVI indicates a much longer growing season than both the MODIS-based LAI estimates and SIF observations. This may be, in part, due to the tendency for NDVI to increase in snowy regions because of spring snowmelt instead of actual vegetation onset [87]. However, the NDVI also implies a longer period of maturity and a later transition in to senescence compared to LAI and SIF, which is most likely due to the maximum-value compositing. Another common occurrence was that SIF observations tended to be phase shifted earlier than LAI observations, which is not surprising since others have reported that changes in vegetation indices can often lag changes in vegetation function (i.e. photosynthesis) [88].

By comparing the regional phenology of a variety of modeled and observed variables we detected ways that the biological strategies built in to the model did not capture the behavior of the real terrestrial biosphere. One common theme was that the model tends to green up during the

spring relatively well compared to observations in many environments, but tends to shift from maturity to senescence late, and the rate of senescence tends to be too slow. Late senescence is a common problem in many terrestrial biosphere models [89], due to the lack of in situ and reliable satellite data. However, because SiB4 phenology is a dynamic and process-driven system, we are able to make inferences about mechanisms causing the model to senesce too late and for too long. We believe that the primary factors causing discrepancies between modeled and observed seasonality are biological functions that SiB4 simply doesn't have. For example, one interpretation is that the model is actually predicting the timing of the shift from maturity to senescence but is missing a critical component: plants are able to cut off nutrient and water flow to their leaves (known as abscission), causing the leaves to brown or fall off more quickly than the modeled leaves, which doesn't include abscission. This would explain why the modeled canopy is green for too long, as indicated by our LAI comparisons.

Another interpretation is that plants have evolved over millions of years to begin shifting their carbon towards roots and reproductive systems, instead of making new leaves, earlier in the year than the weather or climate might require. This may have occurred in plant evolution because particularly bad droughts allowed plants that started senescing early to survive and pass on their genes, while plants that had still been allocating a majority of their carbon towards creating new leaves died out. Therefore, plants may have evolved to be more conservative with their carbon allocation than our model is able to predict using meteorological and climatic factors. Our results would suggest that this is particularly the case in grasses and shrublands because regions dominated by these PFTs tend to have the latest senescence compared to observations.

It should be noted, however, that spring green-up was also late in some environments, such as deciduous broadleaf forests and croplands in the U.S. This may be due to thresholds of light, temperature, and moisture that are too high, causing a late leaf emergence or slow build up of the canopy. Further investigation of the model photosynthesis may shed some light on this issue, by revealing whether the underlying mechanisms of the model carbon allocation, or the model SIF parameterizations are the cause.

We also found that model phenology of croplands works reasonably well in the agricultural center of North America but poorly simulates crop seasonality in other regions of the world. In India, for example, the model reached maturity more than 50 days earlier than observed datasets would indicate. These trends in India can be explained by mistimed planting and harvesting dates of the generic C3 and C4 croplands PFTs in the model. This indicates that SiB4 may need to explicitly represent other major crops, such as rice and sorghum, in future versions in order to accurately capture the phenology and productivity of other agricultural regions around the world.

Bibliography

- [1] Corinne Le Quéré, Michael R Raupach, Josep G Canadell, Gregg Marland, Laurent Bopp, Philippe Ciais, Thomas J Conway, Scott C Doney, Richard A Feely, Pru Foster, et al. Trends in the sources and sinks of carbon dioxide. *Nature geoscience*, 2(12):831, 2009.
- [2] Piers J Sellers, David S Schimel, Berrien Moore, Junjie Liu, and Annmarie Eldering. Observing carbon cycle–climate feedbacks from space. *Proceedings of the National Academy of Sciences*, page 201716613, 2018.
- [3] David Schimel, Britton B Stephens, and Joshua B Fisher. Effect of increasing co2 on the terrestrial carbon cycle. *Proceedings of the National Academy of Sciences*, 112(2):436–441, 2015.
- [4] Helmut Lieth. *Phenology and seasonality modeling*, volume 8. Springer Verlag, Berlin, 1974.
- [5] Andrew D. Richardson, Ryan S. Anderson, M. Altaf Arain, Alan G. Barr, Gil Bohrer, Guangsheng Chen, Jing M. Chen, Philippe Ciais, Kenneth J. Davis, Ankur R. Desai, Michael C. Dietze, Danilo Dragoni, Steven R. Garrity, Christopher M. Gough, Robert Grant, David Y. Hollinger, Hank A. Margolis, Harry McCaughey, Mirco Migliavacca, Russell K. Monson, J. William Munger, Benjamin Poulter, Brett M. Raczka, Daniel M. Ricciuto, Alok K. Sahoo, Kevin Schaefer, Hanqin Tian, Rodrigo Vargas, Hans Verbeeck, Jingfeng Xiao, and Yongkang Xue. Terrestrial biosphere models need better representation of vegetation phenology: results from the north american carbon program site synthesis. *Global Change Biology*, 18(2):566–584, 2012.
- [6] Abraham J Miller-Rushing and Richard B Primack. Global warming and flowering times in thoreau’s concord: a community perspective. *Ecology*, 89(2):332–341, 2008.

- [7] Andrew D Richardson, Trevor F Keenan, Mirco Migliavacca, Youngryel Ryu, Oliver Sonnentag, and Michael Toomey. Climate change, phenology, and phenological control of vegetation feedbacks to the climate system. *Agricultural and Forest Meteorology*, 169:156–173, 2013.
- [8] Mark D Schwartz. Green-wave phenology. *Nature*, 394(6696):839, 1998.
- [9] Nina L Bradley, A Carl Leopold, John Ross, and Wellington Huffaker. Phenological changes reflect climate change in wisconsin. *Proceedings of the National Academy of Sciences*, 96(17):9701–9704, 1999.
- [10] Annette Menzel and Peter Fabian. Growing season extended in europe. *Nature*, 397(6721):659, 1999.
- [11] David S Gill, Jeffrey S Amthor, and F Herbert Bormann. Leaf phenology, photosynthesis, and the persistence of saplings and shrubs in a mature northern hardwood forest. *Tree Physiology*, 18(5):281–289, 1998.
- [12] CK Augspurger, JM Cheeseman, and CF Salk. Light gains and physiological capacity of understorey woody plants during phenological avoidance of canopy shade. *Functional Ecology*, 19(4):537–546, 2005.
- [13] Isabelle Chuine. Why does phenology drive species distribution? *Philosophical Transactions of the Royal Society of London B: Biological Sciences*, 365(1555):3149–3160, 2010.
- [14] Lianhong Gu, Wilfred M Post, Dennis Baldocchi, T Andy Black, Shashi B Verma, Timo Vesala, and Steve C Wofsy. Phenology of vegetation photosynthesis. In *Phenology: An integrative environmental science*, pages 467–485. Springer, 2003.
- [15] Josep Peñuelas and Iolanda Filella. Phenology feedbacks on climate change. *Science*, 324(5929):887–888, 2009.
- [16] Amanda S Gallinat, Richard B Primack, and David L Wagner. Autumn, the neglected season in climate change research. *Trends in Ecology & Evolution*, 30(3):169–176, 2015.

- [17] Anthony L Westerling, Hugo G Hidalgo, Daniel R Cayan, and Thomas W Swetnam. Warming and earlier spring increase western us forest wildfire activity. *science*, 313(5789):940–943, 2006.
- [18] N MacBean, F Maignan, P Peylin, C Bacour, F-M Bréon, and P Ciais. Using satellite data to improve the leaf phenology of a global terrestrial biosphere model. *Biogeosciences*, 12(23):7185–7208, 2015.
- [19] Heikki Hänninen and Karen Tanino. Tree seasonality in a warming climate. *Trends in plant science*, 16(8):412–416, 2011.
- [20] Shilong Piao, Pierre Friedlingstein, Philippe Ciais, Nicolas Viovy, and Jérôme Demarty. Growing season extension and its impact on terrestrial carbon cycle in the northern hemisphere over the past 2 decades. *Global Biogeochemical Cycles*, 21(3), 2007.
- [21] Annette Menzel, Tim H Sparks, Nicole Estrella, Elisabeth Koch, Anto Aasa, Rein Ahas, Kerstin Alm-Kübler, Peter Bissolli, Ol’ga Braslavská, Agrita Briede, et al. European phenological response to climate change matches the warming pattern. *Global change biology*, 12(10):1969–1976, 2006.
- [22] Inés Ibáñez, Richard B Primack, Abraham J Miller-Rushing, Elizabeth Ellwood, Hiroyoshi Higuchi, Sang Don Lee, Hiromi Kobori, and John A Silander. Forecasting phenology under global warming. *Philosophical Transactions of the Royal Society of London B: Biological Sciences*, 365(1555):3247–3260, 2010.
- [23] V Kovalsky and GM Henebry. Alternative methods to predict actual evapotranspiration illustrate the importance of accounting for phenology: the event driven phenology model part ii. *Biogeosciences*, 9:161, 2012.
- [24] Samuel Levis and Gordon B Bonan. Simulating springtime temperature patterns in the community atmosphere model coupled to the community land model using prognostic leaf area. *Journal of Climate*, 17(23):4531–4540, 2004.

- [25] Michael A White, Kirsten M de Beurs, Kamel Didan, David W Inouye, Andrew D Richardson, Olaf P Jensen, JOHN O'KEEFE, Gong Zhang, Ramakrishna R Nemani, Willem JD van Leeuwen, et al. Intercomparison, interpretation, and assessment of spring phenology in north america estimated from remote sensing for 1982–2006. *Global Change Biology*, 15(10):2335–2359, 2009.
- [26] Elsa E Cleland, Isabelle Chuine, Annette Menzel, Harold A Mooney, and Mark D Schwartz. Shifting plant phenology in response to global change. *Trends in ecology & evolution*, 22(7):357–365, 2007.
- [27] Kirsten M De Beurs and Geoffrey M Henebry. Land surface phenology and temperature variation in the international geosphere–biosphere program high-latitude transects. *Global Change Biology*, 11(5):779–790, 2005.
- [28] Jonathan Barichivich, Keith R Briffa, Ranga B Myneni, Timothy J Osborn, Thomas M Melvin, Philippe Ciais, Shilong Piao, and Compton Tucker. Large-scale variations in the vegetation growing season and annual cycle of atmospheric co₂ at high northern latitudes from 1950 to 2011. *Global change biology*, 19(10):3167–3183, 2013.
- [29] Rogier de Jong, Jan Verbesselt, Achim Zeileis, and Michael E Schaepman. Shifts in global vegetation activity trends. *Remote Sensing*, 5(3):1117–1133, 2013.
- [30] Eli K Melaas, Mark A Friedl, and Zhe Zhu. Detecting interannual variation in deciduous broadleaf forest phenology using landsat tm/etm+ data. *Remote Sensing of Environment*, 132:176–185, 2013.
- [31] Bin Tan, Jeffrey T Morisette, Robert E Wolfe, Feng Gao, Gregory A Ederer, Joanne Nightingale, and Jeffrey A Pedelty. An enhanced timesat algorithm for estimating vegetation phenology metrics from modis data. *IEEE Journal of Selected Topics in Applied Earth Observations and Remote Sensing*, 4(2):361–371, 2011.

- [32] Galina Churkina, David Schimel, Bobby H Braswell, and Xiangming Xiao. Spatial analysis of growing season length control over net ecosystem exchange. *Global Change Biology*, 11(10):1777–1787, 2005.
- [33] Alessandro Cescatti, Barbara Marcolla, Suresh K Santhana Vannan, Jerry Yun Pan, Miguel O Román, Xiaoyuan Yang, Philippe Ciais, Robert B Cook, Beverly E Law, Giorgio Matteucci, et al. Intercomparison of modis albedo retrievals and in situ measurements across the global fluxnet network. *Remote sensing of environment*, 121:323–334, 2012.
- [34] Ranga B Myneni, CD Keeling, Compton J Tucker, Ghassem Asrar, and Ramakrishna R Nemani. Increased plant growth in the northern high latitudes from 1981 to 1991. *Nature*, 386(6626):698, 1997.
- [35] Xiaoyang Zhang, Mark A Friedl, Crystal B Schaaf, Alan H Strahler, John CF Hodges, Feng Gao, Bradley C Reed, and Alfredo Huete. Monitoring vegetation phenology using modis. *Remote sensing of environment*, 84(3):471–475, 2003.
- [36] Alemu Gonsamo, Jing M Chen, Chaoyang Wu, and Danilo Dragoni. Predicting deciduous forest carbon uptake phenology by upscaling fluxnet measurements using remote sensing data. *Agricultural and Forest Meteorology*, 165:127–135, 2012.
- [37] Nicolas Delbart, Elisabeth Beaubien, Laurent Kergoat, and Thuy Le Toan. Comparing land surface phenology with leafing and flowering observations from the plantwatch citizen network. *Remote Sensing of Environment*, 160:273–280, 2015.
- [38] C Van der Tol, JA Berry, PKE Campbell, and U Rascher. Models of fluorescence and photosynthesis for interpreting measurements of solar-induced chlorophyll fluorescence. *Journal of Geophysical Research: Biogeosciences*, 119(12):2312–2327, 2014.
- [39] M Meroni, M Rossini, L Guanter, L Alonso, U Rascher, R Colombo, and J Moreno. Remote sensing of solar-induced chlorophyll fluorescence: Review of methods and applications. *Remote Sensing of Environment*, 113(10):2037–2051, 2009.

- [40] Christian Frankenberg, Joshua B Fisher, John Worden, Grayson Badgley, Sassan S Saatchi, Jung-Eun Lee, Geoffrey C Toon, André Butz, Martin Jung, Akihiko Kuze, et al. New global observations of the terrestrial carbon cycle from gosat: Patterns of plant fluorescence with gross primary productivity. *Geophysical Research Letters*, 38(17), 2011.
- [41] Su-Jong Jeong, David Schimel, Christian Frankenberg, Darren T Drewry, Joshua B Fisher, Manish Verma, Joseph A Berry, Jung-Eun Lee, and Joanna Joiner. Application of satellite solar-induced chlorophyll fluorescence to understanding large-scale variations in vegetation phenology and function over northern high latitude forests. *Remote sensing of environment*, 190:178–187, 2017.
- [42] Xing Li, Jingfeng Xiao, and Binbin He. Chlorophyll fluorescence observed by oco-2 is strongly related to gross primary productivity estimated from flux towers in temperate forests. *Remote Sensing of Environment*, 204:659 – 671, 2018.
- [43] Anatoly A. Gitelson, Yi Peng, Jeffery G. Masek, Donald C. Rundquist, Shashi Verma, Andrew Suyker, John M. Baker, Jerry L. Hatfield, and Tilden Meyers. Remote estimation of crop gross primary production with landsat data. *Remote Sensing of Environment*, 121:404 – 414, 2012.
- [44] Yi Peng and Anatoly A. Gitelson. Remote estimation of gross primary productivity in soybean and maize based on total crop chlorophyll content. *Remote Sensing of Environment*, 117:440 – 448, 2012. Remote Sensing of Urban Environments.
- [45] Steven W. Running, Ramakrishna R. Nemani, Faith Ann Heinsch, Maosheng Zhao, Matt Reeves, and Hirofumi Hashimoto. A continuous satellite-derived measure of global terrestrial primary production. *BioScience*, 54(6):547–560, 2004.
- [46] C. J. Tucker and P. J. Sellers. Satellite remote sensing of primary production. *International Journal of Remote Sensing*, 7(11):1395–1416, 1986.

- [47] S.Z. Dobrowski, J.C. Pushnik, P.J. Zarco-Tejada, and S.L. Ustin. Simple reflectance indices track heat and water stress-induced changes in steady-state chlorophyll fluorescence at the canopy scale. *Remote Sensing of Environment*, 97(3):403 – 414, 2005.
- [48] U. Rascher, L. Alonso, A. Burkart, C. Cilia, S. Cogliati, R. Colombo, A. Damm, M. Drusch, L. Guanter, J. Hanus, T. HyvÄrinen, T. Julitta, J. Jussila, K. Kataja, P. Kokkalis, S. Kraft, T. Kraska, M. Matveeva, J. Moreno, O. Muller, C. Panigada, M. Píkl, F. Pinto, L. Prey, R. Pude, M. Rossini, A. Schickling, U. Schurr, D. SchÄjttmeyer, J. Verrelst, and F. Zemek. Sun-induced fluorescence - a new probe of photosynthesis: First maps from the imaging spectrometer hyplant. *Global Change Biology*, 21(12):4673–4684, 2015.
- [49] Jeffrey D. Wood, Timothy J. Griffis, John M. Baker, Christian Frankenberg, Manish Verma, and Karen Yuen. Multiscale analyses of solar-induced fluorescence and gross primary production. *Geophysical Research Letters*, 44(1):533–541, 2017.
- [50] Manish Verma, David Schimel, Bradley Evans, Christian Frankenberg, Jason Beringer, Darren T. Drewry, Troy Magney, Ian Marang, Lindsay Hutley, Caitlin Moore, and Annmarie Eldering. Effect of environmental conditions on the relationship between solar-induced fluorescence and gross primary productivity at an ozflux grassland site. *Journal of Geophysical Research: Biogeosciences*, 122(3):716–733, 2017.
- [51] Xing Li, Jingfeng Xiao, Binbin He, M. Altaf Arain, Jason Beringer, Ankur R. Desai, Carmen Emmel, David Y. Hollinger, Alisa Krasnova, Ivan Mammarella, Steffen M. Noe, PenÄlope Serrano Ortiz, A. Camilo Rey-Sanchez, Adrian V. Rocha, and Andrej Varlagin. Solar-induced chlorophyll fluorescence is strongly correlated with terrestrial photosynthesis for a wide variety of biomes: First global analysis based on oco-2 and flux tower observations. *Global Change Biology*, 24(9):3990–4008, 2018.
- [52] C. Frankenberg, C. O’Dell, L. Guanter, and J. McDuffie. Remote sensing of near-infrared chlorophyll fluorescence from space in scattering atmospheres: implications for its retrieval

- and interferences with atmospheric CO_2 retrievals. *Atmospheric Measurement Techniques*, 5(8):2081–2094, 2012.
- [53] Hualei Yang, Xi Yang, Yongguang Zhang, Mary A Heskell, Xiaoliang Lu, J William Munger, Shucun Sun, and Jianwu Tang. Chlorophyll fluorescence tracks seasonal variations of photosynthesis from leaf to canopy in a temperate forest. *Global change biology*, 23(7):2874–2886, 2017.
- [54] PJ Sellers, YCSY Mintz, YC e al Sud, and A Dalcher. A simple biosphere model (sib) for use within general circulation models. *Journal of the Atmospheric Sciences*, 43(6):505–531, 1986.
- [55] PJ Sellers, DA Randall, GJ Collatz, JA Berry, CB Field, DA Dazlich, C Zhang, GD Collelo, and L Bounoua. A revised land surface parameterization (sib2) for atmospheric gcms. part i: Model formulation. *Journal of climate*, 9(4):676–705, 1996.
- [56] GD v Farquhar, S von von Caemmerer, and JA Berry. A biochemical model of photosynthetic CO_2 assimilation in leaves of C_3 species. *Planta*, 149(1):78–90, 1980.
- [57] G James Collatz, J Timothy Ball, Cyril Grivet, and Joseph A Berry. Physiological and environmental regulation of stomatal conductance, photosynthesis and transpiration: a model that includes a laminar boundary layer. *Agricultural and Forest meteorology*, 54(2-4):107–136, 1991.
- [58] Go J Collatz, M Ribas-Carbo, and JA Berry. Coupled photosynthesis-stomatal conductance model for leaves of C_4 plants. *Functional Plant Biology*, 19(5):519–538, 1992.
- [59] DA Randall, DA Dazlich, C Zhang, AS Denning, PJ Sellers, CJ Tucker, L Bounoua, JA Berry, GJ Collatz, CB Field, et al. A revised land surface parameterization (sib2) for gcms. part iii: The greening of the colorado state university general circulation model. *Journal of Climate*, 9(4):738–763, 1996.

- [60] Ian Baker, A Scott Denning, Niall Hanan, Lara Prihodko, Marek Uliasz, Pier-Luigi Vidale, Kenneth Davis, and Peter Bakwin. Simulated and observed fluxes of sensible and latent heat and co₂ at the wlef-tv tower using sib2. 5. *Global Change Biology*, 9(9):1262–1277, 2003.
- [61] Niall P Hanan, Joseph A Berry, Shashi B Verma, Elizabeth A Walter-Shea, Andrew E Suyker, George G Burba, and A Scott Denning. Testing a model of co₂, water and energy exchange in great plains tallgrass prairie and wheat ecosystems. *Agricultural and Forest Meteorology*, 131(3-4):162–179, 2005.
- [62] Pier Luigi Vidale and R Stöckli. Prognostic canopy air space solutions for land surface exchanges. *Theoretical and applied climatology*, 80(2-4):245–257, 2005.
- [63] IT Baker, L Prihodko, AS Denning, Michael Goulden, S Miller, and HR Da Rocha. Seasonal drought stress in the amazon: Reconciling models and observations. *Journal of Geophysical Research: Biogeosciences*, 113(G1), 2008.
- [64] Ian Timothy Baker. Biophysical behavior in tropical south america. 2011.
- [65] I.T. Baker, A.B. Harper, H.R. da Rocha, A.S. Denning, A.C. Ara-Žjo, L.S. Borma, H.C. Freitas, M.L. Goulden, A.O. Manzi, S.D. Miller, A.D. Nobre, N. Restrepo-Coupe, S.R. Saleska, R. St-ückli, C. von Randow, and S.C. Wofsy. Surface ecophysiological behavior across vegetation and moisture gradients in tropical south america. *Agricultural and Forest Meteorology*, 182-183:177 – 188, 2013.
- [66] Yongjiu Dai, Xubin Zeng, Robert E Dickinson, Ian Baker, Gordon B Bonan, Michael G Bosilovich, A Scott Denning, Paul A Dirmeyer, Paul R Houser, Guoyue Niu, et al. The common land model. *Bulletin of the American Meteorological Society*, 84(8):1013–1024, 2003.
- [67] Kevin Schaefer, A Scott Denning, Neil Suits, Jörg Kaduk, Ian Baker, Sietse Los, and Lara Prihodko. Effect of climate on interannual variability of terrestrial co₂ fluxes. *Global Biogeochemical Cycles*, 16(4), 2002.

- [68] K.D. Haynes, I.T. Baker, A.S. Denning, R. Stockli, K. Schaefer, E.Y. Lokupitiya, and J.M. Haynes. Representing ecosystems using dynamic prognostic phenology based on biological growth stages: Part 1. implementation in the simple biosphere model (sib4). *Journal of Advances in Modeling Earth Systems*, 2018.
- [69] Stan D Wullschleger, Howard E Epstein, Elgene O Box, Eugénie S Euskirchen, Santonu Goswami, Colleen M Iversen, Jens Kattge, Richard J Norby, Peter M van Bodegom, and Xiaofeng Xu. Plant functional types in earth system models: past experiences and future directions for application of dynamic vegetation models in high-latitude ecosystems. *Annals of botany*, 114(1):1–16, 2014.
- [70] Erandathie Lokupitiya, Scott Denning, Keith Paustian, Ian Baker, Kevin Schaefer, Shashi Verma, Tilden Meyers, CJ Bernacchi, Andrew Suyker, and Marc Fischer. Incorporation of crop phenology in simple biosphere model (sibcrop) to improve land-atmosphere carbon exchanges from croplands. *Biogeosciences*, 6(6):969–986, 2009.
- [71] Kevin Schaefer, G James Collatz, Pieter Tans, A Scott Denning, Ian Baker, Joe Berry, Lara Prihodko, Neil Suits, and Andrew Philpott. Combined simple biosphere/carnegie-ames-stanford approach terrestrial carbon cycle model. *Journal of Geophysical Research: Biogeosciences*, 113(G3), 2008.
- [72] Kevin Schaefer, Tingjun Zhang, Andrew G Slater, Lixin Lu, Andrew Etringer, and Ian Baker. Improving simulated soil temperatures and soil freeze/thaw at high-latitude regions in the simple biosphere/carnegie-ames-stanford approach model. *Journal of Geophysical Research: Earth Surface*, 114(F2), 2009.
- [73] Yuri Knyazikhin, Joseph Glassy, J L ; Privette, Yi Tian, Alexander Lotsch, Y Zhang, Yujie Wang, Jeffrey Morisette, Petr Votava, R B ; Myneni, Ramakrishna Nemani, and S W ; Running. Modis leaf area index (lai) and fraction of photosynthetically active radiation absorbed by vegetation (fpar) product (mod15) algorithm theoretical basis document. 01 1999.

- [74] Jorge E Pinzon and Compton J Tucker. A non-stationary 1981–2012 avhrr ndvi3g time series. *Remote Sensing*, 6(8):6929–6960, 2014.
- [75] Ying Sun, Christian Frankenberg, Martin Jung, Joanna Joiner, Luis Guanter, Philipp Köhler, and Troy Magney. Overview of solar-induced chlorophyll fluorescence (sif) from the orbiting carbon observatory-2: Retrieval, cross-mission comparison, and global monitoring for gpp. *Remote Sensing of Environment*, 209:808–823, 2018.
- [76] Bradley C Reed, Michael White, and Jesslyn F Brown. Remote sensing phenology. In *Phenology: An Integrative Environmental Science*, pages 365–381. Springer, 2003.
- [77] Michael A White, Peter E Thornton, and Steven W Running. A continental phenology model for monitoring vegetation responses to interannual climatic variability. *Global biogeochemical cycles*, 11(2):217–234, 1997.
- [78] Christopher A Williams, Niall P Hanan, Jason C Neff, Robert J Scholes, Joseph A Berry, A Scott Denning, and David F Baker. Africa and the global carbon cycle. *Carbon balance and management*, 2(1):3, 2007.
- [79] Q Jane. China: The third pole: Climate change is coming fast and furious to the tibetan plateau, naturenews. *Published online July, 23, 2008*.
- [80] Mingliang Che, Baozhang Chen, John L. Innes, Guangyu Wang, Xianming Dou, Tianmo Zhou, Huifang Zhang, Jianwu Yan, Guang Xu, and Hongwei Zhao. Spatial and temporal variations in the end date of the vegetation growing season throughout the qinghai-tibetan plateau from 1982 to 2011. *Agricultural and Forest Meteorology*, 189-190:81 – 90, 2014.
- [81] Zhoutao Zheng, Wenquan Zhu, Guangsheng Chen, Nan Jiang, Deqin Fan, and Donghai Zhang. Continuous but diverse advancement of spring-summer phenology in response to climate warming across the qinghai-tibetan plateau. *Agricultural and Forest Meteorology*, 223:194 – 202, 2016.

- [82] Lin Zhao, Chien-Lu Ping, Daqing Yang, Guodong Cheng, Yongjian Ding, and Shiyin Liu. Changes of climate and seasonally frozen ground over the past 30 years in qinghai's xizang (tibetan) plateau, china. *Global and Planetary Change*, 43(1):19 – 31, 2004.
- [83] Geli Zhang, Yangjian Zhang, Jinwei Dong, and Xiangming Xiao. Green-up dates in the tibetan plateau have continuously advanced from 1982 to 2011. 110(11):4309–4314, 2013.
- [84] Wenquan Zhu, Nan Jiang, Guangsheng Chen, Donghai Zhang, Zhoutao Zheng, and Deqin Fan. Divergent shifts and responses of plant autumn phenology to climate change on the qinghai-tibetan plateau. *Agricultural and Forest Meteorology*, 239:166–175, 2017.
- [85] A Baccini, N Laporte, SJ Goetz, M Sun, and H Dong. A first map of tropical africa's above-ground biomass derived from satellite imagery. *Environmental Research Letters*, 3(4):045011, 2008.
- [86] Xiangming Xiao, Stephen Hagen, Qingyuan Zhang, Michael Keller, and Berrien Moore III. Detecting leaf phenology of seasonally moist tropical forests in south america with multi-temporal modis images. *Remote Sensing of Environment*, 103(4):465–473, 2006.
- [87] Nicolas Delbart, Laurent Kergoat, Thuy Le Toan, Julien Lhermitte, and Ghislain Picard. Determination of phenological dates in boreal regions using normalized difference water index. *Remote Sensing of Environment*, 97(1):26–38, 2005.
- [88] Pablo J Zarco-Tejada, Arturo Morales, Luca Testi, and Francisco J Villalobos. Spatio-temporal patterns of chlorophyll fluorescence and physiological and structural indices acquired from hyperspectral imagery as compared with carbon fluxes measured with eddy covariance. *Remote Sensing of Environment*, 133:102–115, 2013.
- [89] James T Randerson, Forrest M Hoffman, Peter E Thornton, Natalie M Mahowald, Keith Lindsay, Yen-Huei Lee, Cynthia D Nevison, Scott C Doney, Gordon Bonan, Reto Stöckli, et al. Systematic assessment of terrestrial biogeochemistry in coupled climate–carbon models. *Global Change Biology*, 15(10):2462–2484, 2009.